Journal of South American Earth Sciences 52 (2014) 149–165

Contents lists available at ScienceDirect

Journal of South American Earth Sciences

journal homepage: www.elsevier.com/locate/jsames

Holocene ochreous lacustrine sediments within the Famatina Belt, NW Argentina: A natural case for fossil damming of an acid drainage system

Santiago N. Maza [a,b,*], Gilda Collo [a], Ricardo A. Astini [a], Fernando Nieto [c], José Miguel Nieto [d]

[a] Laboratorio de Análisis de Cuencas, CICTERRA – Universidad Nacional de Córdoba, Av. Vélez Sarsfield 1611, 2° piso, of.7, X5016GCA Córdoba, Argentina
[b] Departamento de Aplicadas, Universidad Nacional de La Rioja, L.M. de La Fuente s/n, La Rioja, Argentina
[c] Departamento de Mineralogía y Petrología and I.A.C.T., Universidad de Granada – CSIC, Avda. Fuentenueva s/n, 18002 Granada, Spain
[d] Departamento de Geología, Universidad de Huelva, Campus 'El Carmen', 21071 Huelva, Spain

ARTICLE INFO

Article history:
Received 2 October 2013
Accepted 28 February 2014

Keywords:
Acid rock drainage
Ochreous sediments
Quaternary paleolake deposits
Schwertmannite
Jarosite
Landslide-dammed lakes

ABSTRACT

A 44 m-thick lacustrine succession of silty-clay banded ochres and subordinated sandstones, and conglomerates (known as the Corral Amarillo Formation) is superbly exposed within the Famatina Belt (Central Andes of Argentina) after deep entrenchment by the present-day Amarillo river due to strong recent uplifting and consequent relative drop in base level. The unusual ochreous-rich succession was produced by natural damming (3.48–3.54 ^{14}C kyr BP) of an acid drainage system linked to the alteration cap of polymetallic deposits. Facies of silty-clay ochre (wet season) and banded ochre (dry season) from the paleolacustrine setting are composed of jarosite + goethite and goethite respectively. Geochemically, these layers record high concentrations of Fe_2O_3 (25–55 wt. %) and trace elements (Cu, Zn, Co, As, and Mo with mean concentrations of 2759; 2467; 109; 375 and 116 ppm, respectively). Their origin is inferred from a comparative analysis with the present-day Amarillo river, which has a pH of ~3, $(SO_4)^{2-}$ concentrations of ~5000 mg/l, and jarosite as the dominant phase, in the upper catchments. Waters downstream have pH values of 3–4.5, $(SO_4)^{2-}$ concentrations of ~3000–480 mg/l, and schwertmannite as the dominant phase. Thus goethite in the paleolake facies is likely related to schwertmannite transformation by an aging process, whereas jarosite is probably transported from the river but could also be associated with post-depositional formation regulated by variations in grain size and the pore fluid chemistry. The Corral Amarillo Formation offers a Natural model, which may be employed to infer the effect on nature of acid drainage of mineralized areas.

1. Introduction

Acid drainage related to the oxidation of sulfide ore deposits either natural (acid rock drainage: ARD) or originated from mining activities (acid mine drainage: AMD) has been widely recognized as a major environmental problem in terrestrial aquatic ecosystems around the world (Bowell and Bruce, 1995; Cornell and Schwertmann, 1996; Nordstrom and Alpers, 1999; Dold, 2010). Sulfide oxidation is complex and its effects can vary depending on the geology, climate, and microbiology of a given region (Acero et al., 2006). However, the integrated study of rivers associated with ARD provides means of understanding various physical, chemical, and biological processes that control its formation and spatio-temporal variations. This understanding is essential for the control and remediation of ARD environmental impacts. Ochreous precipitates associated with ARD/AMD (e.g., schwertmannite, jarosite, goethite) effectively trap trace elements, and thereby attenuate dissolved metals generated by these systems (Bigham et al., 1992; Jambor and Blowes, 1994; Nordstrom and Alpers, 1999).

In the central region of the Famatina Belt (Central Andes of Argentina), side-canyon rock avalanches naturally dammed the middle stretch of the Amarillo river, creating temporary lakes, during Holocene time. The river headwaters drain an important

* Corresponding author. CICTERRA – CONICET – Universidad Nacional de Córdoba, Av. Vélez Sarsfield 1611, Edificio CICTERRA, X5016GCA Córdoba, Argentina.
E-mail addresses: santiagomaz@gmail.com (S.N. Maza), gcollo@efn.uncor.edu (G. Collo), raastini@efn.uncor.edu (R.A. Astini), nieto@ugr.es (F. Nieto), jmnieto@uhu.es (J.M. Nieto).

http://dx.doi.org/10.1016/j.jsames.2014.02.010
0895-9811/

alteration halo of high-sulfidation epithermal deposits (Au–Cu–Ag–As–Sb) and Cu and Mo porphyries in the Nevados de Famatina mining district (NFMD; Losada-Calderon and McPhail, 1994; Pudack et al., 2009). The Amarillo river is characterized by acidic waters and widespread deposition of ochreous sediments along its banks. The lacustrine sediments consist of more than 44 m of rhythmic silty-clay ochres and subordinated iron-rich sandstones, conglomerates, and breccias, and are known as the Corral Amarillo Formation (Limarino et al., 1994, Fig. 1). This unit is exceptionally preserved as elevated terraces at both sides of the river, which form a canyon about 2 km long. The ochreous sediments in this lacustrine succession represent an almost unique example of ancient sedimentation associated with ARD, in this case linked to the Neogene uplift of the Famatina Belt and the progressive unroofing of high-sulfidation mineralization. In addition, the Amarillo river drainage system was impacted by mining activities between 1890 and 1925 (La Mejicana mine).

In this contribution, mineralogical and geochemical analyses from the fine-grained distal paleolake deposits are presented and compared with the alluvial sediments of the modern Amarillo river. These data allow an understanding of the evolution of the acid drainage system taking place nowadays along the Amarillo river

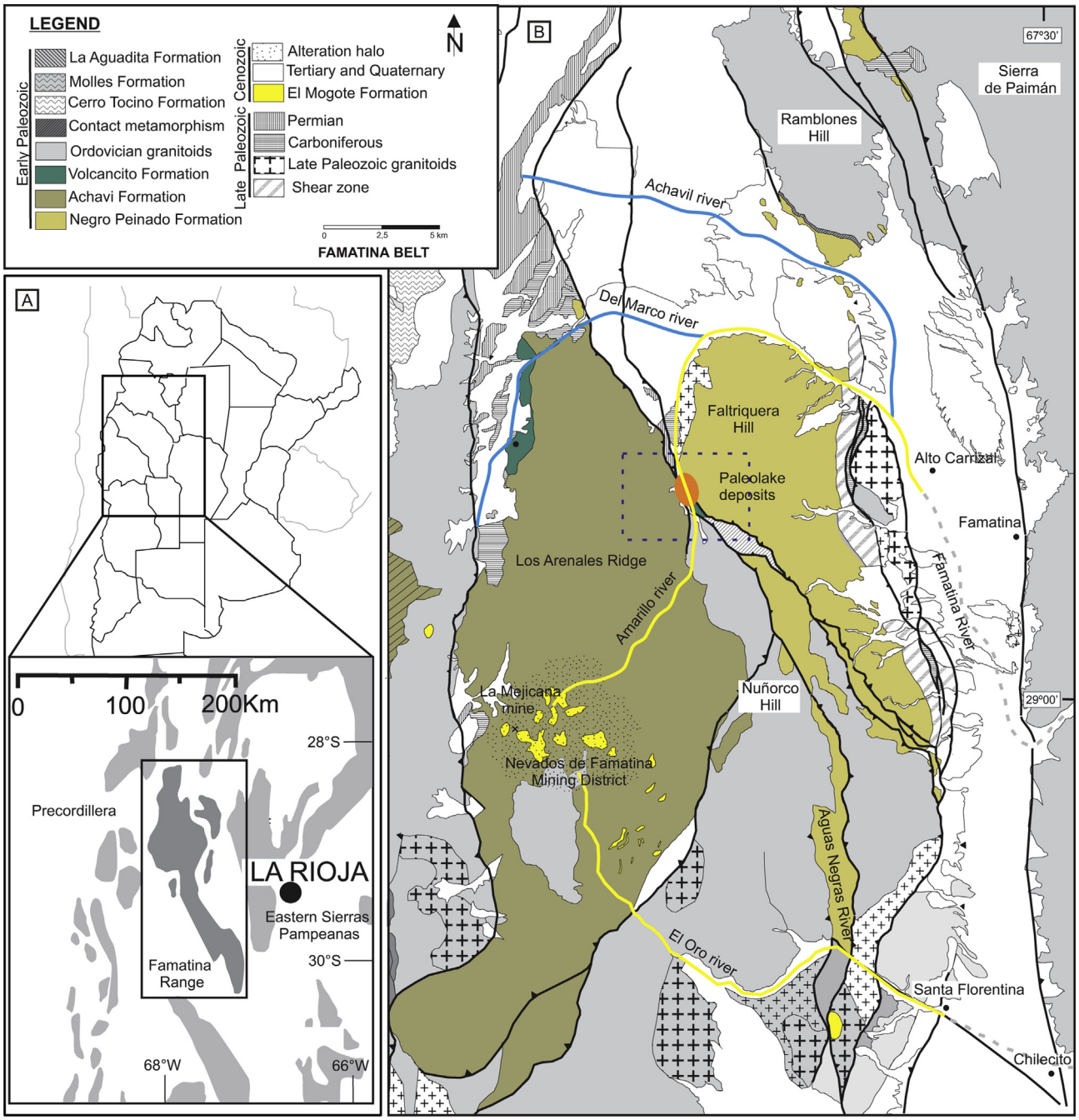

Fig. 1. A) Map of Argentina showing the study area. B) Geological map of the central region of the Famatina Belt. The rectangle shows the location of the lake deposits (modified from Collo et al., 2009). Yellow rivers indicated acid drainage, whereas blue rivers show circumneutral waters. (For interpretation of the references to colour in this figure legend, the reader is referred to the web version of this article.)

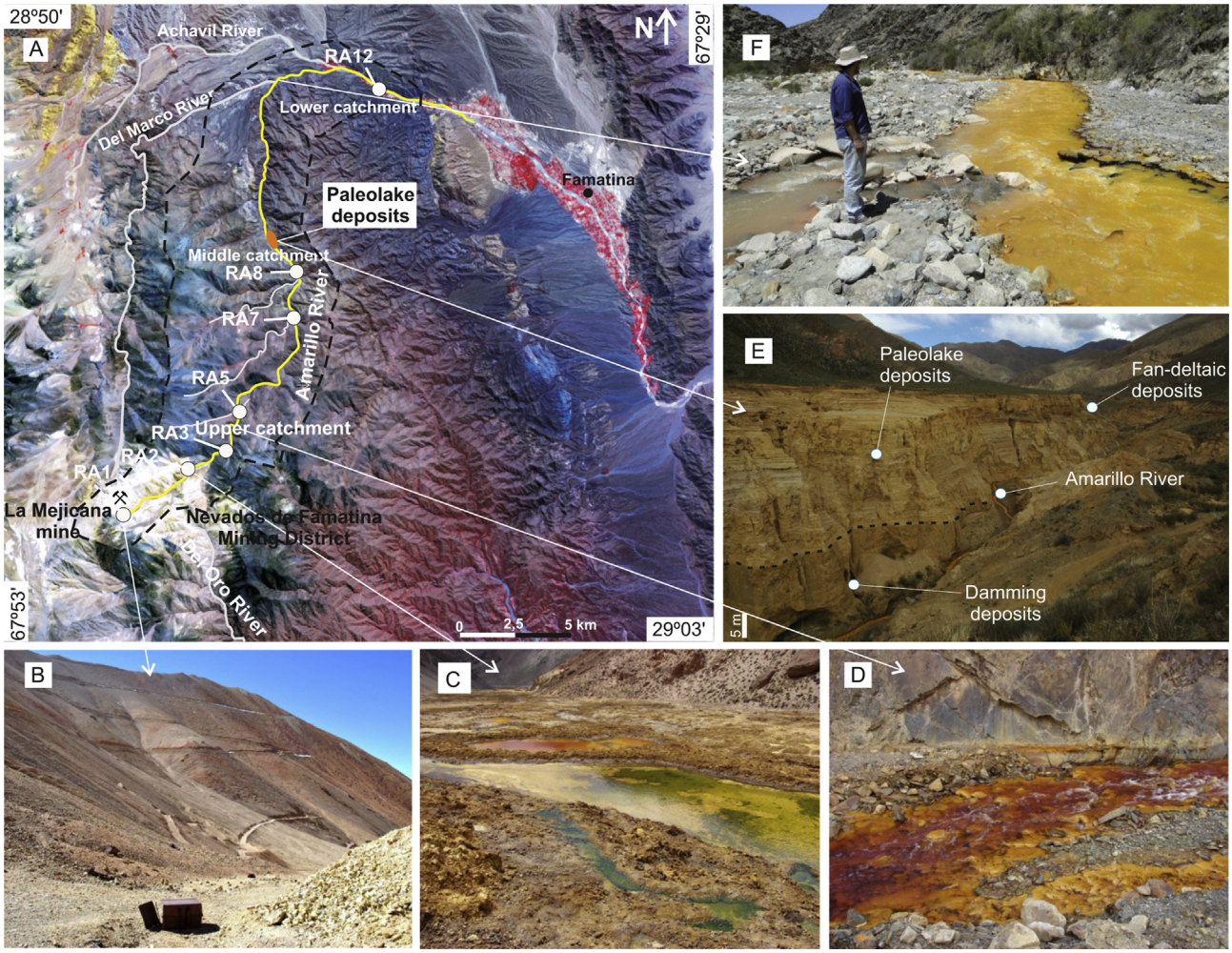

Fig. 2. A) Satellite image from the central Famatina Belt, showing the upper, middle, and lower course of the Amarillo river. B) Detail of the La Mejicana mining area, where the waste rocks and galleries are located. C) Detail of the region with emerging waters that generate swamping, creating the headwaters of the Amarillo river. D) Amarillo river bed in the upper basin with yellowish-red waters and secondary precipitated sediments. E) Detail of the canyon with lacustrine deposits from the Corral Amarillo Formation. F) Confluence between the Amarillo and Del Marco rivers.

and suggest two genetic models for the ochreous sediments from the Holocene Corral Amarillo Formation. The results also highlight the fact that this paleolake deposit constitutes an excellent record for understanding the behavior of natural acid systems. Additionally, the Corral Amarillo deposits could serve as a natural analogue of anthropogenic acid rock drainage.

2. Geological framework

The Famatina Belt, located between 27° and 31° south latitude, is part of the current broken foreland of the Sierras Pampeanas in the Central Andes of Argentina (Dávila and Astini, 2007). The basement of the region consists of Ordovician granites (Pankhurst et al., 1998; Dahlquist and Alasino, 2005), which intrude low-grade metamorphic Cambrian host rocks (Negro Peinado and Achavil Formations, Collo et al., 2009, 2011), unconformably covered by an Ordovician marine volcano-sedimentary series (Volcancito Formation, Astini, 2003). The early Paleozoic series are unconformably overlain by Pennsylvanian continental arkoses and widespread Permian red beds (Agua Colorada and De La Cuesta formations; Limarino et al., 2010). Covering the Paleozoic rocks lays a thick, synorogenic Tertiary siliciclastic succession that records the complex Neogene uplift. At this time and associated with subduction flattening (Dávila et al., 2004), dacites (known as the Mogote Formation, De Alba, 1954; Turner, 1971) were intruded. Magmatic activity began 5.0 ± 0.3 Ma ago, and ended with several stages of hydrothermal differentiation at 3.8 ± 0.2 Ma (Losada-Calderon et al., 1994). Molybdenum-copper-gold mineral deposits developed associated with the dacite intrusion and with complex hypabyssal-hydrothermal polymetallic processes, along with more distal epithermal Cu–Au (Ag–As–Sb–Te) veins, usually radiating from fault zones (Pudack et al., 2009). Within the La Mejicana area (Fig. 1), pyrite is the most abundant hypogenic mineral, associated with enargite, famatinite, tetrahedrite-tennantite, chalcopyrite, sphalerite, and galena (among others) as subordinate phases (Brodtkorb and Schalamuk, 1999). The secondary supergene mineralization developed in a leaching-oxidation zone extending from the surface to a depth of 192 m (average of 10–35 m, Lurgo Mayón, 1999). The transition to the cementation zone, where limonite coexists with jarosite, goethite, and ferrimolybdite (and hematite to a lesser extent), is sharp. In the subsurface, the supergene mineralization is directly related to the hypogenic copper sulfides, with chalcocite as the main mineral and subordinated covellite. The supergene alteration covers a large area but is vertically shallow. It consists of argilitization, limonitization caps, probable sericitization, and is closely related to pyrite and the

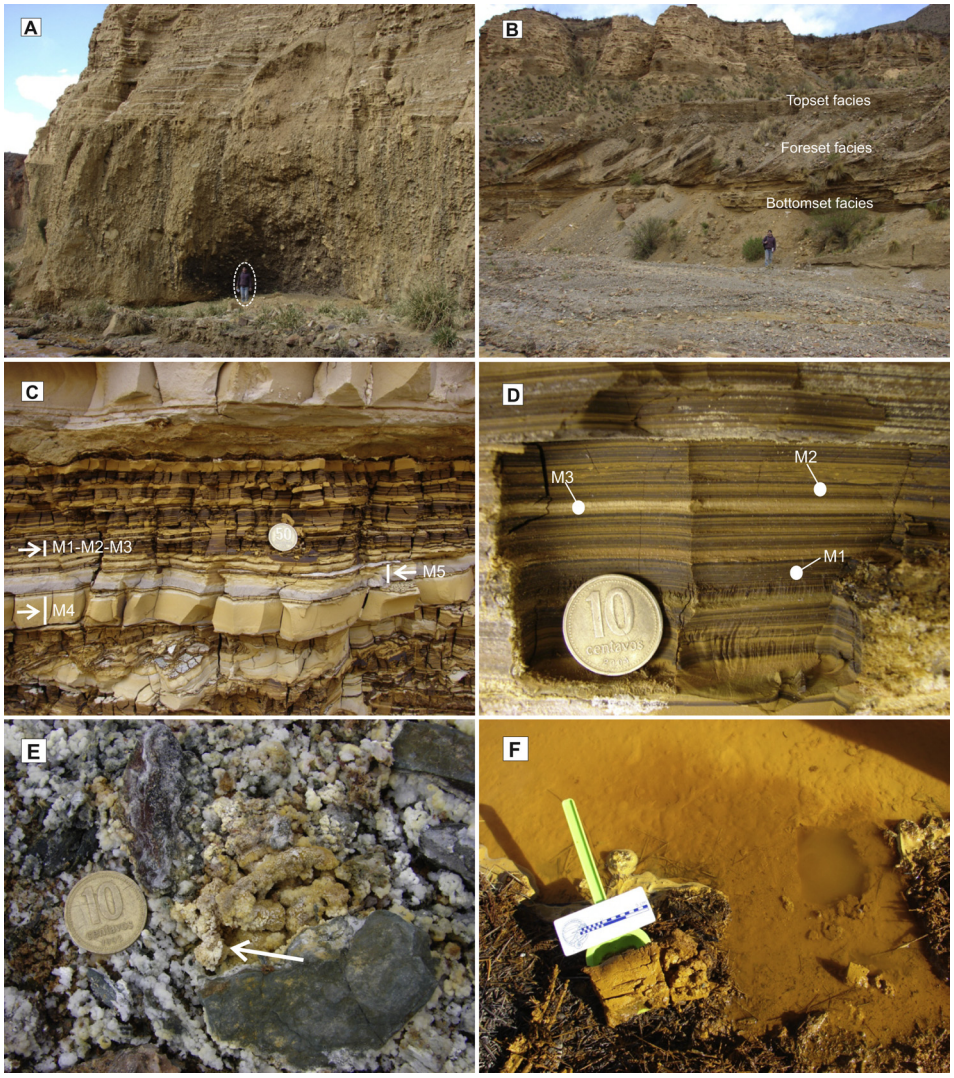

Fig. 3. A) Image of the contact between the dam and the lacustrine deposits. B) Gravel delta deposits where the division between top, fore, and bottomset facies is recognized. C and D) Distal lake deposits; note the rhythmicity, variation in thickness, and arrangement of the banded ochre (M1, M2, and M3), silty-clay ochre (M4), and silty-sandy (M5) facies. E and F) Detailed photos of different types of sediments associated with the acid drainage of the Amarillo river.

permeability of the previously altered rock (Lurgo Mayón, 1999). In the La Mejicana area, a leaching-oxidation zone represented by a gossan has been reported (Brodtkorb and Schalamuk, 1999), with a widespread alunite-kaolinite alteration zone.

At present, the ranges are surrounded by Early Pleistocene consolidated polymictic conglomerates related to uplifted terraces (Cueva de Pérez Formation, Marcos and Zanettini, 1982; Pudack et al., 2009), and by thick Quaternary alluvial fans partly entrenched in their proximal regions due to continuous, rapid uplift. This recent uplift has created a steep marked relief over 6200 m above sea level (m a.s.l.), which has in turn unroofed the mineralized Miocene intrusives.

The Quaternary lacustrine deposits of the Corral Amarillo Formation (Turner, 1960, 1971; Limarino et al., 1994) crop out in the middle reach of the Amarillo river drainage basin, at 2750 m a.s.l. The deposits comprise shales, sandstones, breccias, and conglomerates with significant secondary iron ochres either as cements or as continuous layers forming the bulk of the succession (Fig. 2). They are located south of the fold-and-thrust belt within the Famatina region (Fig. 1). Maza (2009) carried out a detailed paleoenvironmental analysis in this unit, recognizing five environmentally significant primary facies associations: (1) dam deposits, (2) delta plain gravel-rich deposits, (3) pro-delta deposits and proximal lacustrine deposits, (4) deep lacustrine (distal) deposits, and (5) marginal lacustrine deposits (Fig. 3A, B, C).

Recently, Maza et al. (2011b) reported an absolute radiocarbon age for organic matter preserved in finer levels of the paleolake, according to which sedimentation of paleolacustrine deposits started between 3.48 and 3.54 ^{14}C kyr BP. Therefore, the damming event that led to the paleolake formation may be linked to regional episodes already recorded in northwestern Argentina (Hermanns and Strecker, 1999, 2004, 2006), and it coincides with the avalanche cluster associated with the Titicaca wet period (<5.0 kyr BP; cf. Trauth and Strecker, 1999; Hermanns et al., 2000; Trauth et al., 2000).

2.1. The Amarillo river system

The current Amarillo river system is endorheic as a consequence of low rainfall, a high evaporation index, and an intermontane basins development. The area is subject to a continental high-mountain dry climate, with around 200 mm year^{-1} of rainfall,

mainly between January and March (62%), and frequent flash flooding. During the winter, there are infrequent snowfalls and snowmelt is negligible. The Amarillo river (35 km in length) has a drainage basin of 155 km^2, and an average discharge rate of ~0.5 m^3/s during the dry season (April–December) in the lower catchment. During the summer, the average flow rate is ~2.0 m^3/s (Maza et al., 2011a). This high-mountain river has turbulent yellow waters carrying large amounts of dissolved metals that exceed water-quality standards by several orders of magnitude (Fernández-Turiel et al., 1995; WHO, 2004; CAA, 1994, Fig. 2). This high concentration of metals and its acidity is the result of the oxidative dissolution of pyrite and other sulfides in its headwaters (NFMD). This process produces a low pH, releasing potentially toxic elements for being transported downstream (España et al., 2005; Acero et al., 2006; Asta et al., 2010). Significantly, within the mining area, there are no discharges of acidic waters into the Amarillo river from tailing material (dumps), waste rock, or galleries. Furthermore, the material extracted from the La Mejicana mine was sent via a cableway system to Chilecito, a town located several kilometers east, where the ore was processed (see Fig. 1).

3. Methodology

3.1. Field site and sampling

The paleolake succession and the bed sediments of the present-day Amarillo river were sampled during the dry season (October-2008). In the Corral Amarillo Formation, the sampling was conducted along existing river terraces by rappelling to 17 points, spaced an average of 2.5 m apart vertically down the 44 m of the unit. Ochreous and siliciclastic levels corresponding to the distal paleolake deposits were sampled at each point (Fig. 2). In addition, the bed sediments, efflorescences, and waters from the present-day Amarillo river and its tributaries were sampled at seven points to evaluate their characteristics (Fig. 2 and Table 1):

- RA1 is at 4600 m a.s.l. and upstream of the La Mejicana mine, with no influence from mining activity. The water was frozen over and salt precipitates were abundant. At 0.6 km below this point, water inflows and rises the surface again around 4.71 km downstream (RA2).
- RA2 is at 3869 m a.s.l. and downstream of the underground mine workings. It is a swampy area, with small interconnected pools, abundant algae growth, sediments, and salt precipitates (Fig. 2C).
- RA3 is at 3865 m a.s.l. in the first stretch of the river in the upper catchment (Fig. 2D).
- RA5 (3427 m a.s.l.), RA7 (2964 m a.s.l.), and RA9 (2839 m a.s.l.) are in the Amarillo river's middle reach and correspond to points with circumneutral water (from the west) joining the main course. Sediment samples were collected before the confluence of the two streams, at the confluence, and beyond it.
- RA12 (1979 m a.s.l.) is located between the Alto Carrizal and Los Corrales, below the confluence of the Amarillo river with the Del Marco (Fig. 2F) and Achavil rivers.

pH was measured in situ in the Amarillo river (Table 1).

3.2. Analytical methods

The mineralogy of the bulk rock and the <2 μm fraction was determined by X-ray diffraction (XRD) with a PANalytical X'Pert PRO diffractometer. The bulk-rock measurements were carried out on unoriented samples of distal sediments from the Corral Amarillo Formation and bed sediments from the present-day Amarillo river. Conditions were 40 kV and 40 mA, at a scan rate of 1°min^{-1} between 3° and 60° 2θ and specifically between 3° and 40° 2θ for iron oxide/hydroxide/sulfate bulk rock samples. Samples were dried at room temperature, and ~10 g were powdered in an agate mortar. The mineralogy of the <2 μm fraction was determined in five layers, from ochre and silty-sandy facies from the Corral Amarillo Formation. Samples were treated, separated, and mounted in oriented aggregates following the recommendations of Moore and Reynolds (1997).

The geochemistry of the paleolake sediments was determined for 37 samples of silty-clay ochre facies and silty-sandy facies taken in pairs. Major and trace-element concentrations of the lacustrine phases and alluvial sediment were determined by X-ray fluorescence using a BRUKER S4 EXPLORER device. Laboratory preparation consisted in separating 15 g of material using a plastic spatula and then pulverizing it in an agate mortar. The samples were calcined at 900 °C for 1 h to determine the LOI.

4. Lithofacies of the deep lacustrine (distal) facies association

Characteristic features of this facies association are the remarkably tabular geometry and lateral continuity of beds and bedding planes, the sharp contacts, and well-consolidated structure, with an absence of flow indicators (e.g., absence of mechanical structures). Microloading features are rare and always accompany slight normal grading. Bathymetric indicators that might allow water-depth determination were not found, but no wave-ripple features or surface traction deposits have been recorded. Few coarse-grained graded-laminated beds indicate hyperpycnal bottom-layer deposits, but most of the even-bedded muds seem to be consistent with settling in a relatively calm deep lacustrine environment. Moreover, the absence of desiccation cracks, evaporitic levels or eolian features (Rogers and Astin, 1991) reinforce the interpretation of sedimentation under a stable water body, below the influence of the wave-base and beyond the direct control of a fan-deltaic system preserved at the proximal extent. Based on the projection of the thickness of inclined bedding in the adjacent Gilbert-type fore-sets, a minimum water depth of 1–5 m can be inferred for deposition (Postma and Roep, 1985).

Table 1
Sediment and water sampling from the Amarillo river bed (1/11/2008).

Sampling point	Sample	Latitude	Longitude	Elevation	pH	T
		S	W	(m a.s.l.)		°C
RA1	Water and efflorescences	29°01'00.9''	67°46'59.3''	4600	3.26	4.9
RA2	Water, bedrock sediments, crusts, and efflorescences	28°59'51.6''	67°44'21.4''	3869	3.00	9.6
RA3	Water and bedrock sediments	28°59'48.9''	67°43'57.2''	3825	2.93	9.6
RA5	Water, bedrock sediments, crusts, and efflorescences	28°58'34.6''	67°42'53.3''	3427	2.93	9.3
RA7	Water, bedrock sediments, crusts, and efflorescences	28°56'25.9''	67°40'52.2''	2963	3.20	15.1
RA8	Water, bedrock sediments, crusts, and efflorescences	28°55'33.2''	67°40'32.9''	2835	3.33	5.7
RA12	Water and bedrock sediments	28°50'50.8''	67°37'17.7''	1979	4.45	15.5

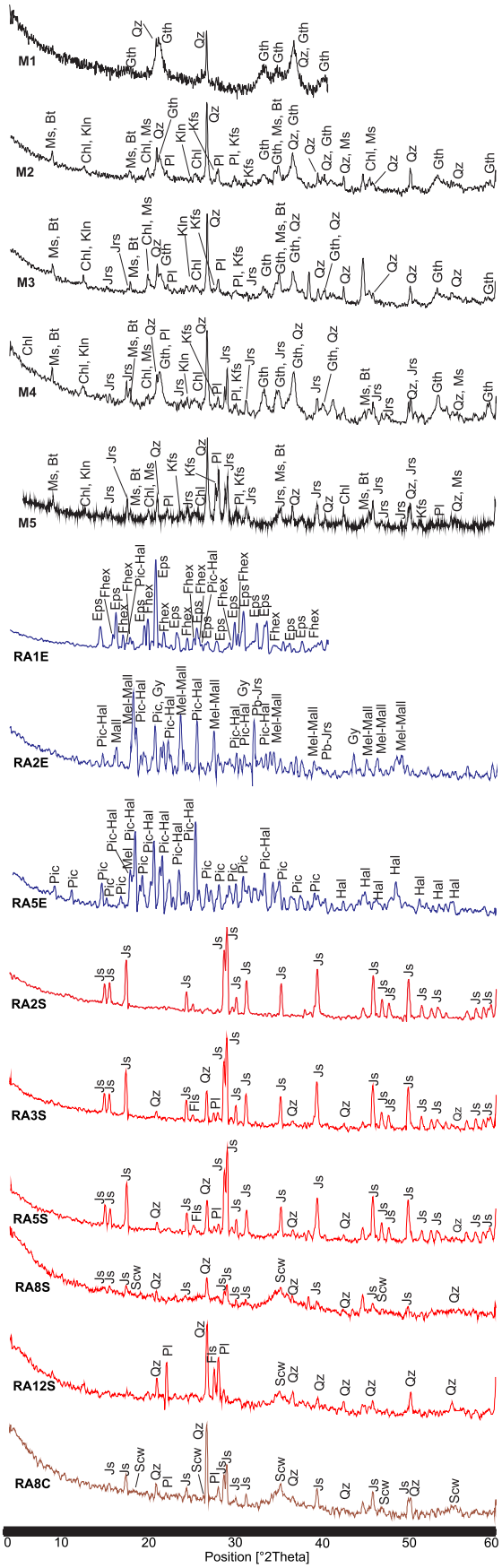

This association comprises three facies: (1) *Banded ochre facies.* It is composed of tabular, very thin layers (<1–4 cm), with a high proportion of iron oxides (see Fig. 3D). Internally, they have delicate parallel lamination comprising dark brown laminas (M1), intense orangish-yellow laminae (M2), and less frequently slightly reddish-gray laminae (M3). This facies is interpreted as calm-water vertical fallout deposits (settling) given their great lateral continuity, fine grain size, and internal structures, and in some levels it is affected by synsedimentary microfolding. (2) *Silty-clay ochre facies.* It comprises massive tabular layers (4–6 cm thick), with marked lateral continuity and sharp contacts (M4). The coloring of internal layers ranges from orange to yellow or gray depending on the proportions of iron minerals. Remains of well-preserved plants, stems, leaf cuticles and diatoms (identified in SEM images) are common. Based on their remarkable lateral continuity, very fine grain size, and massive structure, this is interpreted as diluted residual dense flows with settling of varying proportions of iron minerals. (3) *Silty-sandy facies*. It has marked tabularity, lateral continuity of layers (M5), and a gray color. Bed thickness ranges from 2 to 20 cm (commonly 5–7 cm). There is granular grading to massive texture, a notable absence of tractive structures, and whitish precipitates such as hard crusts and plant remains. Powdery orange nodules ~2 mm in diameter are common. This facies is consistent with hyperpycnic flow deposits, most probably associated to flood events within the feeding river system.

5. Mineralogical and geochemical characterization

5.1. Mineralogical analysis of the lacustrine deposits from the Corral Amarillo Formation

In the banded ochre facies (usually with millimetric-scale lamination) dark-brown layers (M1), yellowish layers (M2), and grayish layers (M3) were analyzed. Massive yellowish centimetric layers (M4) from the silty-clay ochres and grayish centimetric to decimetric layers (M5) from silty-sandy facies were also studied (see Fig. 3C and D).

5.1.1. Whole-rock mineralogy

The M1 layers contain almost exclusively goethite as the only iron mineral phase and lesser amounts of quartz. In the M2 layers, goethite is accompanied by detrital silicate phases, mainly quartz, muscovite, plagioclase, potassium feldspar, biotite, chlorite, and kaolinite. These same minerals appear to be dominant in the M3 layers, with minor goethite and jarosite. In the M4 and M5 layers (lighter-colored), the predominance of sulfated phases is diagnostic (Fig. 4). In the silty-clay ochres (M4), jarosite and goethite predominate, with smaller proportions of silicate phases. In the silty-sandy facies (M5), the mineralogy consists of jarosite, quartz, muscovite, plagioclase, potassium feldspar, and biotite, with subordinate chlorite, kaolinite, and smectites. Spherical orange nodules approximately 2–10 mm in diameter are fairly common; X-ray patterns display typical jarosite reflections. Given the large nodule size, they likely formed in situ, with the clay minerals providing the K^+ needed for jarosite formation (Taylor, 1996; Caraballo et al., 2011).

Mineral associations are common in systems with acidic aqueous chemistry, where iron oxides/hydroxides and sulfates/hydroxysulfates are secondary (authigenic) and related to oxidation

Fig. 4. XRD diagrams of representative samples from the M1, M2, and M3 layers within the banded ochre facies, M4 in the silty-clay ochre facies, and M5 in the silty-sandy facies; and patterns from representative samples of salt efflorescence and bottom sediments in the upper, middle, and lower Amarillo river course.

Table 2
Major elements in lacustrine sediments are expressed as wt. %. Fe contents are expressed as Fe^{+3}.

Detection limit	SiO_2	Al_2O_3	Fe_2O_3	CaO	Na_2O	K_2O	MgO	TiO_2	MnO	P_2O_5	SO_3	LOI
	%											
17-M5	42.5	14.9	12.1	0.6	0.9	5.3	1.7	0.7	0.1	0.1	7.8	13.0
16-M5	47.5	16.3	10.3	0.8	1.2	3.8	2.4	0.7	0.1	0.1	3.9	12.6
15-M5	49.1	17.8	8.4	0.3	1.0	4.8	1.8	0.7	0.1	0.2	3.2	12.3
14-M5	49.0	18.5	7.8	0.4	0.9	4.8	2.0	0.7	0.1	0.1	2.7	12.7
13-M5	52.2	20.6	6.3	0.5	1.0	4.8	2.3	0.9	0.1	0.2	1.0	9.8
12-M5	50.9	20.3	7.7	0.3	0.9	4.7	2.2	0.8	0.1	0.2	1.3	10.3
11-M5	42.7	17.0	15.3	0.3	0.8	4.9	1.9	0.8	0.1	0.1	4.1	13.1
10-M5	46.9	17.2	12.0	0.7	1.0	4.0	2.1	0.7	0.1	0.2	2.4	12.5
9-M5	52.7	20.5	8.9	0.3	0.9	5.0	2.1	0.8	0.1	0.2	0.8	9.1
8-M5	50.9	20.6	8.0	0.3	0.9	5.1	2.3	0.8	0.2	0.1	1.3	9.2
7-M5	53.9	20.4	9.4	0.2	0.8	5.2	2.0	0.8	0.2	0.2	0.2	9.4
6-M5	53.6	19.0	5.6	0.7	1.1	4.3	2.7	0.8	0.1	0.1	1.2	10.6
5-M5	58.1	17.8	6.0	0.7	1.3	3.9	2	0.9	0.1	0.2	1.7	7.1
3-M5	44.6	20.9	4.6	0.3	0.7	3.9	2.1	0.7	0.1	0.1	3.9	17.8
2-M5	45.4	15.6	11.0	1.0	1.1	3.1	2.3	0.7	0.1	0.1	4.0	15.4
1-M5	59.5	18.0	8.7	0.7	1.2	4.0	1.5	1.0	0.1	0.2	0.3	4.6
17-M4	33.6	12.2	22.5	0.3	0.8	4.2	1.5	0.5	0.1	0.4	6.5	17.2
16-M4	26.3	11.1	41.6	0.1	0.4	2.5	0.9	0.4	0.05	0.3	2.2	14.0
15-M4	9.3	3.6	24.8	0.1	0.2	6.6	0.4	0.1	0.02	0.04	19.9	34.9
14-M4	41.1	16.0	23.1	0.2	0.7	4.0	1.7	0.6	0.1	0.3	1.4	10.6
13-M4	29.0	11.3	32.3	0.1	0.6	2.8	1.2	0.5	0.1	0.3	3.3	18.3
12-M4	36.0	13.8	29.4	0.1	0.6	3.4	1.4	0.6	0.1	0.3	1.9	12.1
11-M4	26.0	10.8	34.2	0.1	0.5	3.4	1.1	0.4	0.1	0.2	5.4	17.4
10-M4	34.8	14.8	29.3	0.1	0.5	3.6	1.4	0.5	0.1	0.3	1.9	12.3
8-M4	45.9	18.2	15.9	0.1	0.6	4.9	1.9	0.7	0.2	0.2	1.7	9.4
7-M4	12.0	5.3	29.5	0.03	0.3	5.3	0.4	0.2	sd	0.2	16.5	30.1
6-M4	38.4	15.0	24.4	0.1	0.6	3.9	1.9	0.6	0.1	0.3	2.2	12.2
5-M4	24.4	9.5	38.8	0.6	0.4	1.9	0.8	0.3	0.1	0.1	3.6	19.3
4-M4	38.9	14.7	23.2	0.2	0.7	3.1	1.5	0.6	0.1	0.2	2.8	13.2
3-M4	36.1	16.7	16.7	0.2	0.6	2.9	1.5	0.5	0.1	0.1	4.3	19.7
2-M4	35.0	13.9	23.5	0.4	0.7	2.9	1.3	0.5	0.1	0.1	3.3	18.4
1-M4	44.9	16.8	20.2	0.2	0.7	3.9	1.2	0.7	0.04	0.2	1.1	10.1
7-M1	10.8	5.5	56.4	0.1	0.3	1.2	0.5	0.2	0.5	0.2	3.5	20.7

and leaching/dissolution of pyrite and other sulfides. Silicates are generally associated with the catchment's detrital contribution, but many clays can also form in that environment (Fernández-Remolar et al., 2011). Hematite as a dominant phase of the ochre deposits (as inferred by Limarino et al. (1994)) was not confirmed during this investigation.

5.1.2. Mineralogy of the <2 μm fraction

XRD analysis of this fraction provided details on the clay mineralogy, as well as established the occurrence of other fine-grained and possibly authigenic phases. In the M1 layer, only goethite and quartz were recognized. In the M2 layer, illite was identified in addition to quartz and goethite. In the M3 layer, goethite concentrations are lower, and smectites and kaolinite were recognized as well as quartz and illite. In the M4 layer, illite, smectites, and kaolinite occur with minor quartz and goethite. In the M5 layer, accessory chlorite was identified in addition to the M4 minerals.

The mineralogy of the <2 μm fraction is consistent with the bulk-rock composition, with variable amounts of iron hydroxides and iron hydroxysulfates in the M1, M2, and M4 layers, and a predominance of clay phases such as smectites and kaolinite in the M3 and M5 layers. Preliminary chemical analyses by scanning electron microscopy and transmission electron microscopy (SEM and TEM, Wunderlin et al., in press) indicate that the expandable clays are predominantly nontronite in the ochre layers and beidellite and montmorillonite in the M3 and M5 layers. Based on textural relations, the first is interpreted as authigenic phases wrapping iron aggregates, whereas the latter may have a detrital origin related to the argillic alteration zones in the system headwaters.

5.2. Geochemical analysis of the Corral Amarillo Formation lacustrine deposits

The geochemical analysis revealed the chemical composition of the relatively deep (distal) lacustrine succession and the compositional variations of major and trace elements along the 44 m of stratigraphic column. M4 (silty-clay ochre facies) and M5 (silty-sandy facies) layers were discriminated to compare the chemical compositions of the two contrasting levels recorded throughout the sequence. A sample from an M1 layer (in banded ochre facies) was selected due to its particular mineralogical composition and position in the sequence. The iron is the major chemical component the all the M4 layers (15.9–41.5 wt. % Fe_2O_3), whereas M1 present the highest values (56.3 wt. % Fe_2O_3). In samples from the M5 layers the Fe_2O_3 content (4.6–15.3 wt %) is significantly lower than in the M1 and M4 ochre layers (Table 2). In these three layers (M1, M4, and M5), SO_3 concentrations are similar at 2.5–4.9 wt. %. Only two M4 samples show higher concentrations of SO_3 (~17 wt. %). In the overall sequence, and particularly in the ochre layers, Fe/S ratios are higher than the ratio derived from pyrite oxidation (FeS_2) suggesting that SO_4 would be lost from the system during transport or aging processes. The other major elements have higher average concentrations in M5 layers (50 wt. % SiO_2, 18.5 wt. % Al_2O_3, 4.5 wt. % K_2O, 2.1 wt. % MgO, 0.5 wt. % Na_2O, and 1 wt. % CaO) than in the M4 layers (32 wt. % SiO_2, 12.7 wt. % Al_2O_3, 3.7 wt. % K_2O, 1.3 wt. % MgO, 0.6 wt. % Na_2O, and 0.2 wt. % CaO), and in the M1 layer (10.8 wt. % SiO_2, 5.5 wt. % Al_2O_3, 1.2 wt. % K_2O, 0.5 wt. % MgO, 0.3 wt. % Na_2O, and 0.1 wt. % CaO).). These elements show a negative correlation with Fe_2O_3 (see Fig. 5). Minor elements such as Ti, P, and Mn show a similar trend in the M5 layers (average of 0.8 wt. % TiO_2, 0.2 wt. % P_2O_5, and 0.1 wt. % MnO), except for Mn, which is slightly

Table 3
Trace elements in lacustrine sediments are expressed as ppm.

Detection limit	Ba	Sr	Zr	Rb	Zn	V	Cr	Cu	Y	Ni	Pb	Ga	Co	As	Mo
	ppm														
17-M5	520	140	195	173	135	120	77	144	19	nd	nd	nd	29	nd	nd
16-M5	480	126	181	157	297	nd	97	153	23	36	79	nd	29	nd	nd
15-M5	550	103	171	197	200	nd	99	135	22	38	60	24	nd	nd	21
14-M5	560	104	166	202	147	120	115	149	24	43	115	23	nd	nd	nd
13-M5	580	105	202	216	187	140	83	128	26	45	98	27	nd	nd	nd
12-M5	590	88	172	217	222	nd	113	135	28	50	133	27	nd	nd	nd
11-M5	520	80	174	182	171	nd	121	116	23	36	nd	nd	nd	nd	nd
10-M5	500	125	173	172	215	nd	77	130	26	41	107	nd	27	nd	nd
9-M5	640	77	179	219	208	130	91	109	28	49	nd	27	8	nd	nd
8-M5	640	92	186	214	242	nd	126	125	38	58	82	26	nd	nd	nd
7-M5	660	56	181	228	259	nd	120	119	25	49	nd	26	37	nd	nd
6-M5	692	130	191	183	380	nd	102	154	34	45	172	26	17	nd	nd
5-M5	550	131	213	164	557	nd	113	93	33	64	nd	nd	nd	nd	nd
3-M5	510	87	133	203	1226	nd	84	181	29	81	235	24	23	nd	nd
2-M5	450	138	157	136	418	nd	74	219	18	44	98	nd	28	nd	nd
1-M5	610	154	321	182	243	nd	114	129	27	38	91	nd	34	nd	nd
17-M4	420	74	110	128	137	94	81	204	10	46	nd	nd	nd	nd	nd
16-M4	340	48	76	130	266	nd	107	203	12	nd	218	nd	nd	230	99
15-M4	nd	27	25	36	37	nd	nd	49	nd	nd	nd	nd	nd	nd	nd
14-M4	520	88	129	191	265	140	104	167	21	50	131	nd	44	205	46
13-M4	400	63	87	128	204	nd	117	180	19	nd	81	nd	nd	nd	55
12-M4	495	75	106	164	209	nd	100	151	16	nd	81	nd	109	231	67
11-M4	390	76	73	134	241	150	68	193	8	nd	209	nd	nd	375	92
10-M4	440	93	106	180	356	nd	104	218	19	nd	170	nd	nd	255	72
8-M4	617	64	146	220	281	nd	131	135	26	63	76	nd	nd	nd	nd
7-M4	250	51	34	124	87	132	50	159	nd	nd	116	nd	nd	343	116
6-M4	430	46	137	183	403	nd	103	214	23	46	229	nd	63	217	68
5-M4	260	27	50	70	397	nd	68	205	14	nd	nd	nd	nd	nd	nd
4-M4	400	45	135	147	2467	150	85	2759	23	81	nd	nd	nd	nd	50
3-M4	410	48	91	142	1528	nd	88	268	21	78	169	nd	58	nd	29
2-M4	340	28	70	111	410	nd	84	235	14	nd	nd	nd	nd	nd	nd
1-M4	490	56	136	187	232	nd	111	237	13	nd	75	nd	nd	nd	21
7-M1	nd	nd	26	43	349	nd	103	221	nd	nd	nd	nd	nd	361	85

higher in M1 (0.5 wt. % MnO) (see Table 2). The LOI contents are higher in the M1 layer (average of 20.7 wt. % in M1, 16.8 wt. % in M4, and 11 wt. % in M5).

In the silty-sandy facies, trace elements such as Ba, Rb, Zr, Sr, Cr, V, and Y (average concentrations of 566, 190, 187, 108, 100, 32, and 26 ppm, respectively) show negative correlation with Fe and higher contents than in the M1 and M4 layers (Table 3). Furthermore, Ga and Nb appear only in the silty-sandy layers (mean concentrations of 26 and 16 ppm, respectively). Mo and Co show positive correlation with Fe contents (Fig. 5), whereas Cu, Zn, Pb, and Ni have similar contents in silty-sandy facies and do not show correlation with Fe contents (Fig. 5). Iron concentrations decrease towards the top of the stratigraphic column both in the M4 and M5 layers (Fig. 6). This is consistent with the progressive increase in silty-sandy facies (where iron concentrations are lower) upsequence, associated with the coarsening trend (see Fig. 6). Moreover, the Si + Al distribution shows negative correlation to that of iron (with values increasing upsequence; Fig. 6). Ochre layers are generally richer in transition metals (Fe, Co, Ni, Cu, Zn, Mo, and Pb) than the silty-sandy facies, where alkali and alkaline metals and metalloids are dominant (e.g., Na, K and Rb, Mg, Ca, Sr, and Si).

5.3. The present-day Amarillo river

5.3.1. Water characterization

The present-day Amarillo river changes in discharge, color, and water chemistry from upstream in the NFMD mineralized zone to the downstream town of Famatina. In the upper catchment, waters shift from colorless/green (at points RA2 and RA3) to red (at points RA5–RA7), with a pH of 3.2–2.9, respectively (Table 1 and Figs. 2C and D and 7). In the middle catchment (point RA8), the river waters are yellow, with a pH of 3.3 (Table 1 and Figs. 2C and D and 7). These variations are related to the buffering effects promoted by the iron species, which can control the pH at acidic conditions through the hydrolysis reaction of the ferric cation [$Fe^{3+} + 3H_2O = Fe(OH)_3(s) + 3H^+$] (Gómez et al., 2004; Fernández-Remolar et al., 2008), by the precipitation of ochreous sediments on the riverbed (as has been observed), and by the confluence of tributaries along its course. Data from this study also reveal the limited capacity for neutralization of the geological materials (e.g. limestone), of the confluence of rivers, and of biological factors within the study area.

The western tributaries (sampled at points RA5, RA7, and RA8) represent about one-quarter of the flow of the Amarillo river (pH of 6.5–7.5, Fig. 7). At the confluence points, these streams create local changes, increasing the pH in all cases. This sudden change in pH induces precipitation of yellowish to greenish sediments. However, a few meters below the confluence, the color and pH of the Amarillo river are both restored. On the other hand, the confluence of the Amarillo river with the Achavil and del Marco rivers (the two largest tributaries, Fig. 2F) in the lower drainage basin produces permanent changes consisting of more precipitates, an increase in pH (~4.5), and a dilution of dissolved metal concentrations.

Maza et al. (2011a) and Lecomte et al. (2014) show that dissolved iron concentrations reach a peak of >1200 mg/l downstream of the La Mejicana mine but decrease to 0.12 mg/l in the lower drainage basin (RA12). They also concluded that sulfate has a similar trend, with dissolved concentrations of ~5241 mg/l downstream of the mine and ~480 mg/l in the lower catchment. Trace elements also have high concentrations upstream and decrease downstream. These conclusions determined extremely high total dissolved solids (TDS) in the uppermost catchments and relatively lower TDS downstream.

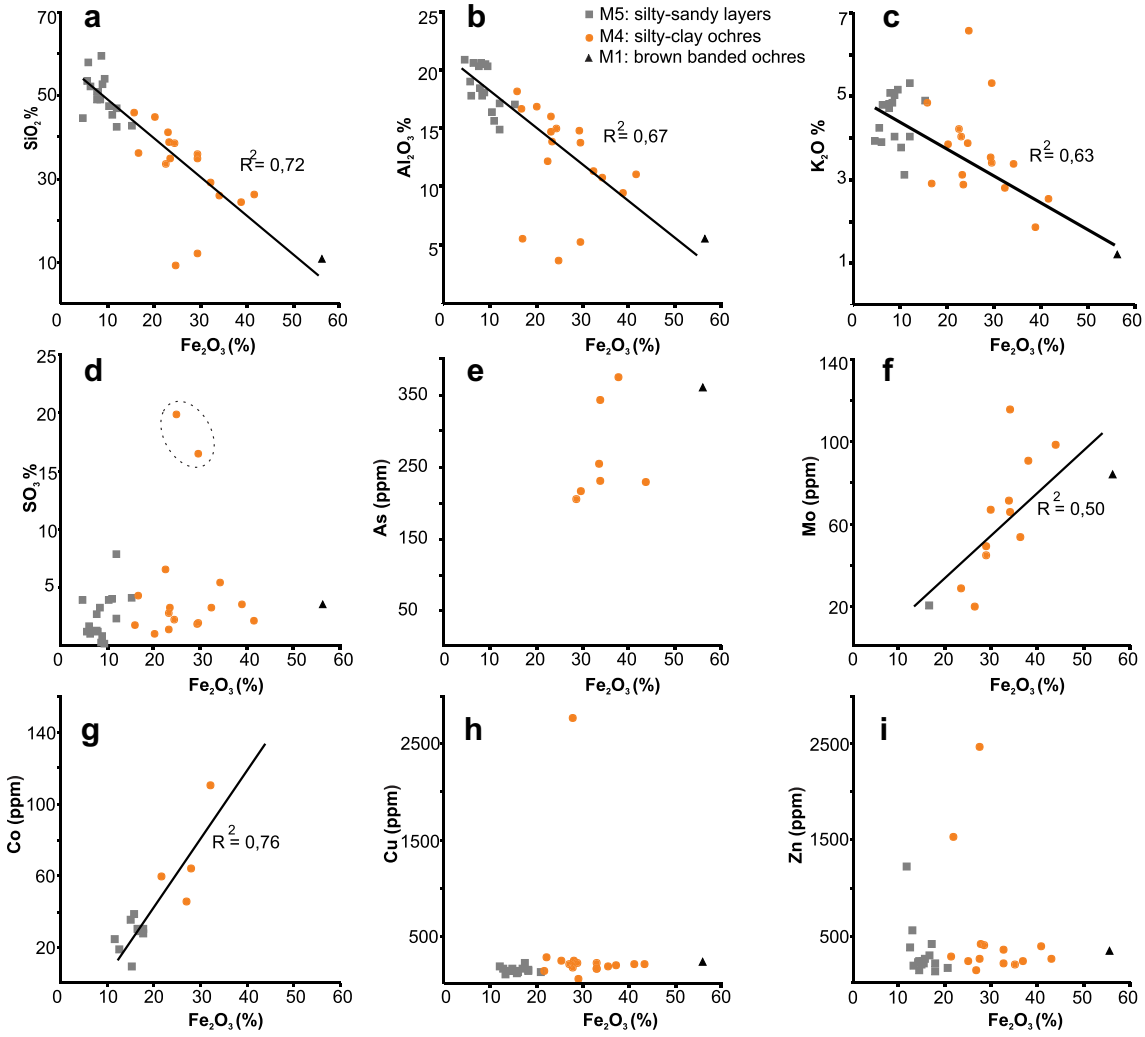

Fig. 5. A, B, C, and D) Relationship between Fe_2O_3 and the major oxides in lacustrine sediments. In D, two samples with anomalous SO_3 values are shown with dotted lines. E, F, G, H, and I) Diagrams showing the relationship between Fe and trace elements (values expressed in wt. %). Gray squares refer to M5 layers; orange circles the M4 layers, and black triangles the M1 layer. The trend line is presented only in diagrams with $R^2 > 0.5$. (For interpretation of the references to colour in this figure legend, the reader is referred to the web version of this article.)

5.3.2. Mineralogy of associated sediments

Fieldwork and mineral analysis on sediment samples along the catchment of the Amarillo river indicate at least three types of precipitates:

1. *Efflorescent Sulfate Salts.* These salts appear as greenish and bluish precipitate blankets in springs and pools in the uppermost catchment (RA1 and RA2) and less frequently as whitish coatings on the river banks (RA3 to RA8; Fig. 3D). Sample RA1E, upstream of the La Mejicana mine, comprises mainly the epsomite salt series, together with smaller amounts of ferrohexahydrite, and pickeringite-halotrichite. Sample RA2E, downstream of the mine, consists mainly of the melanterite hydrated sulfate group, with predominant melanterite and mallardite, with accompanying pickeringite-halotrichite and plumbojarosite, and minor gypsum (Fig. 4). Sample RA5E, on the river bank near RA5, presents pickeringite-halotrichite group salts, with smaller amounts of melanterite. Recognized minerals generally have good crystallization and a predominance of Mg–Al phases over Fe^{+2} phases. Analyses also show that the more dehydrated series predominate downstream.
2. *Bed sediments.* These sediments are ferruginous yellowish-green precipitates with a soft to spongy consistency with varying proportions of detrital siliciclastic material. They cover the riverbed along the entire length of the Amarillo river (RA2 to RA12, Fig. 3E). RA2S shows an absolute predominance of jarosite (Fig. 4); in RA3S and RA5S, jarosite also dominates but with the subordinate participation of detrital minerals such as quartz, plagioclase, and feldspar. A large number of reflections with sharp peaks indicates that these phases generally have well-developed crystals. The analyses of bed sediment samples from the middle and lower catchments show that RA8S and RA12S are mainly schwertmannite with subordinate jarosite. Detrital minerals such as quartz, plagioclase, and feldspar increase in concentration downstream in these sediments (Fig. 4). Sample RA5U (mainly schwertmannite) belongs to the greenish precipitates found at the confluence of the Amarillo river with one of its tributaries (pH of 3.4). Downstream of the confluence, river conditions are quickly restored (pH ~3) and predominant jarosite. It is noteworthy that XRD analysis on a sediment sample from an artisanal evaporation ponds near the paleolake deposits downstream of RA8 shows a predominance of schwertmannite with subordinate jarosite. These sediments

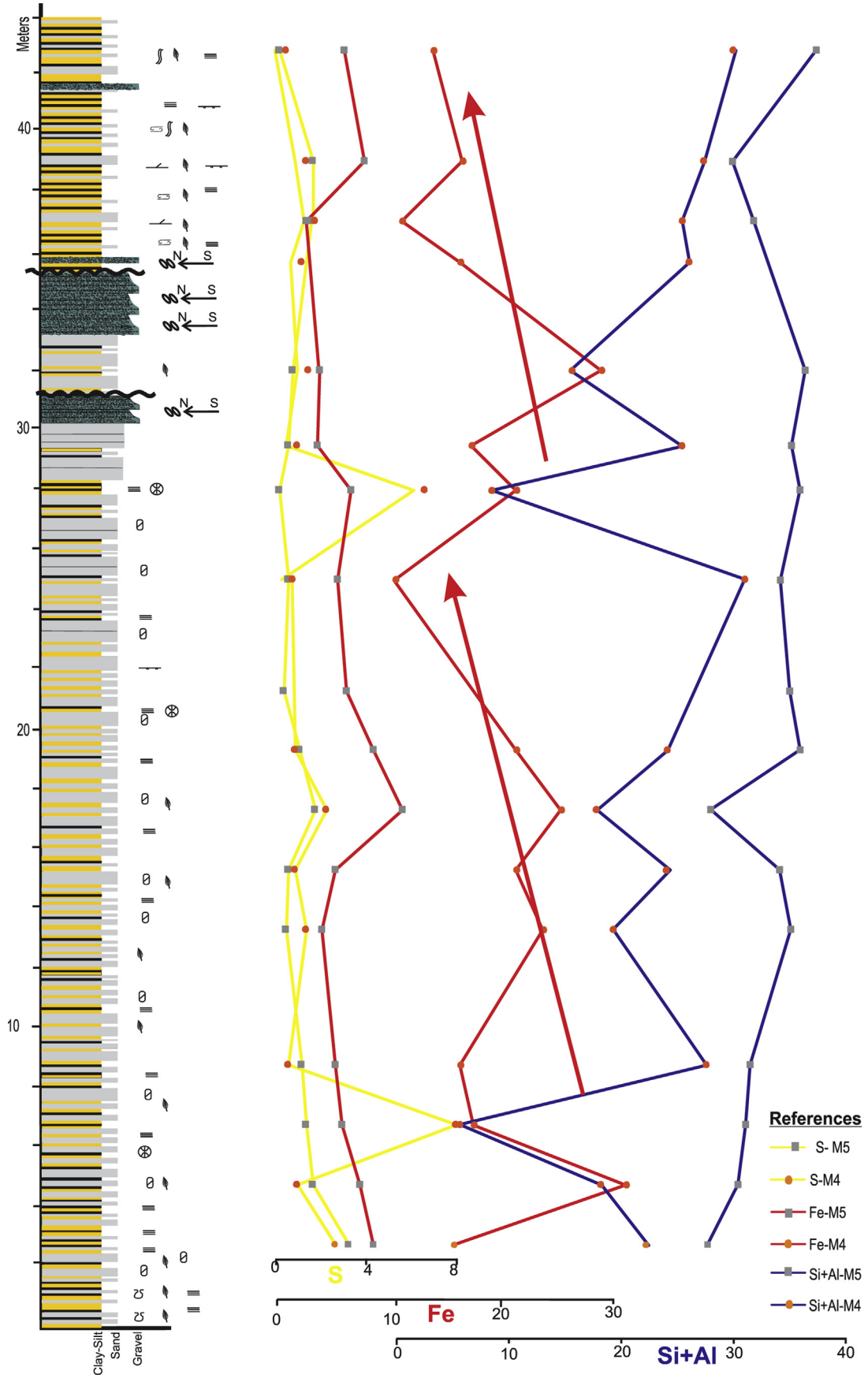

Fig. 6. Major element geochemistry variation along the stratigraphic column of the distal paleolake deposits.

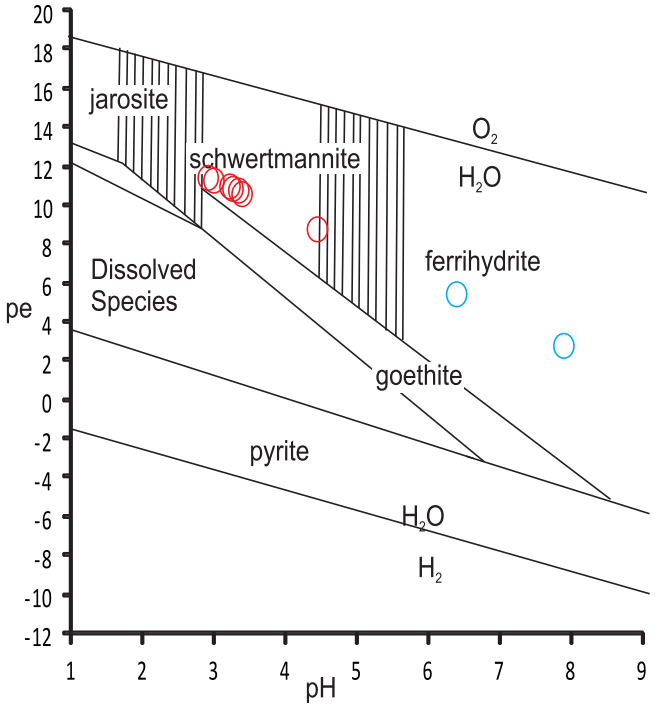

Fig. 7. pe-pH diagram for Fe–S–K–O–H system at 25 °C modified from Bigham et al. (1996). Fields of metastability are shown by dashed lines. Values of pe (calculated with PHREEQ-C) and pH from water samples along the river (red circles) and from tributaries (blue circles) are shown. Progressively higher pH values correspond to more distal samples. (For interpretation of the references to colour in this figure legend, the reader is referred to the web version of this article.)

comprise thin dark laminated layers over massive yellowish sediments. In all the XRD analyses on the current bed sediments, iron oxides/hydroxides such as hematite, goethite, ferrihydrite, or lepidocrocite were not found, although their presence in small amounts cannot be discarded.

3. *Dark crusts.* These crusts are gel-like brownish to blackish ferruginous precipitates coating bed sediments in small pools or clasts near river banks with aerial exposure. They are found mainly in the upper part of the stream as far down as the paleolake deposits (RA3 to RA8). XRD analysis (RA8C, RA7C, and RA5C) reveals predominant schwertmannite and jarosite in similar proportions, with subordinate silicate minerals.

5.3.3. Geochemistry of associated sediments

Tables 4 and 5 give the concentrations for major and trace elements of the Amarillo river present-day ochre deposits associated with acid drainage. Geochemical analyses show high concentrations of Fe_2O_3 and SO_3 in the bed sediments along the entire river channel. Fe_2O_3 contents increase from ~27.5 wt. % in the headwaters to ~43.7 wt. % in the middle stretch and 24.9 wt. % in the lower drainage basin; however, sulfite decreases downstream (from ~22.1 wt. % to ~10.7 wt. %). SiO_2, Al_2O_3, MgO, Na_2O, and CaO contents are very low. Some trace elements in the bed sediments (Cu, Zn, As, and Mo) have very high concentrations and are associated with sulfur, decreasing downstream. Some of these elements reach extremely high concentrations in the efflorescences (Zn > 14,000 ppm, Cu > 5000 ppm, and As >1300 ppm, Table 5). Concentrations of metal, particularly Cu, Zn, As and Mo are generally similar than those reported for Fe-rich precipitates in other sites (Webster et al., 1998; Childs et al., 1998; Hudson-Edwards et al., 1999).

6. Genesis of the ochreous sediments

6.1. The current ochre from the Amarillo river drainage basin

The analysis of present-day sediments and waters of the Amarillo river shed light on the processes and factors involved in the iron minerals precipitation. Iron precipitates formation depends on the pH, SO_4^{2-} concentrations, and metal availability, which act as limiting factors in the prevalence of iron sulfate/hydroxysulfates or iron oxides/hydroxides in sediments (Fig. 7; Bigham et al., 1990, 1994; Cornell and Schwertmann, 1996; Asta et al., 2010). Additionally, in fluvial metal transportation systems, the coagulation is a required intermediate step between precipitation and settling (Boult, 1996).

The mineralogical distribution of sulfate phases in bed sediments during the dry winter season is directly related to pH and water chemistry in each stretch. The uppermost catchment is the

Table 4
Values of major oxides in sediments of the Amarillo river expressed in wt. %.

Detection limit	SiO_2	Al_2O_3	Fe_2O_3	CaO	Na_2O	K_2O	MgO	TiO_2	MnO	P_2O_5	SO_3	LOI
	%											
RA1E	8.5	4.1	2.6	0.8	0.6	0.9	9.7	0.1	2.2	0.1	29.4	39.3
RA5E	5.2	16.0	3.7	0.5	0.3	1.0	2.6	0.1	4.5	0.1	53.4	10.0
RA2aS	0.6	1.2	27.5	0.1	0.1	4.6	0.1	0.01	0.1	0.4	22.1	42.8
RA2bS	0.7	0.3	27.8	0.01	0.3	6.9	nd	0.01	nd	0.3	24.7	38.9
RA3S	5.3	1.7	29.1	0.1	0.2	7.2	0.1	0.1	0.01	0.3	24.0	31.6
RA5S-au	9.9	3.4	30.1	0.1	0.3	6.8	0.3	0.2	0.02	0.2	22.5	25.9
RA5aS-u	0.9	0.9	44.2	0.1	nd	0.1	0.2	0.01	0.03	0.1	13.5	39.8
RA5bS-u	19.3	6.8	36.7	0.1	0.4	3.8	0.3	0.3	0.02	0.2	11.4	20.6
RA5S-du	8.1	2.8	30.3	0.1	0.3	6.6	0.3	0.2	0.02	0.2	22.9	28.0
RA7S	29.9	10.7	24.6	0.2	0.5	4.4	1.2	0.5	0.1	0.2	11.1	16.5
RA7S-u	0.7	0.5	45.3	0.1	nd	0.2	0.1	0.02	0.01	0.1	13.5	39.4
RA8S	2.6	0.9	43.7	0.1	nd	0.8	0.1	0.1	0.02	0.2	15	36.4
RA8S-Ca	17.3	5.7	29.7	0.3	0.4	3.8	0.6	0.3	0.03	0.3	15.7	25.6
RA12S	26.1	15.2	24.9	0.8	0.7	2.4	0.7	0.5	0.1	0.2	10.7	17.5
RA2C	0.8	1.3	21.9	0.2	0.2	4.8	0.2	nd	0.1	0.2	23.5	46.7
RA7C	13.7	4.7	32	0.2	1.5	3.1	2.0	0.3	0.05	0.2	17.9	24.0
RA7C-du	10.1	4.0	40.3	0.2	0.2	1.1	0.4	0.2	0.03	0.1	13.3	30.0
RA8C	18.4	5.6	36.0	0.4	0.7	2.5	0.7	0.4	0.05	0.2	14.1	20.8
Min	0.6	0.3	2.6	0.04	0.1	0.1	0.1	0.01	0.01	0.1	10.7	10.0
Mean	9.9	5.7	29.5	0.2	0.4	3.4	1.2	0.2	0.4	0.2	19.9	29.6
Max	29.9	16	45.3	0.8	1.5	7.2	9.7	0.5	4.5	0.4	53.4	46.7

Table 5
Values of trace elements in sediments of the Amarillo river expressed in ppm.

Detection limit	Ba	Sr	Zr	Rb	Zn	V	Cr	Cu	Y	Ni	Pb	Co	As	Mo
	ppm													
RA1E	nd	15	33	42	12810	nd	nd	199	17	26	56	20	nd	nd
RA5E	nd	Nd	33	39	14710	nd	nd	5381	42	335	nd	56	nd	nd
RA2aS	nd	27	nd	35	321	165	32	584	nd	nd	nd	nd	1300	448
RA2bS	nd	53	nd	97	Nd	nd	nd	323	nd	nd	nd	nd	400	164
RA3S	nd	58	46	88	58	83	nd	478	nd	nd	nd	nd	590	283
RA5S-au	270	47	72	110	207	329	62	440	nd	nd	nd	nd	265	62
RA5aS-u	nd	Nd	nd	nd	177	298	29	217	nd	nd	nd	nd	255	50
RA5bS-u	nd	56	51	131	107	143	nd	527	3	nd	nd	nd	461	182
RA5S-du	nd	55	50	125	90	151	53	504	nd	nd	nd	nd	454	177
RA7S	410	43	145	167	166	295	58	252	15	nd	nd	58	269	38
RA7S-u	nd	Nd	nd	nd	48	130	93	142	nd	nd	nd	58	nd	19
RA8S	nd	Nd	nd	nd	Nd	293	56	143	nd	nd	nd	nd	301	46
RA8S-ca	290	71	96	109	101	281	42	272	9	nd	nd	nd	303	70
RA12S	404	352	194	129	156	nd	121	681	22	nd	nd	nd	nd	Nd
RA2C	nd	38	nd	52	511	69	nd	633	nd	nd	nd	nd	317	153
RA7C	230	48	90	110	110	384	55	241	8	nd	nd	nd	344	78
RA7C-du	nd	69	nd	62	122	121	77	212	nd	nd	nd	171	nd	Nd
RA8C	290	81	142	104	96	nd	92	216	nd	nd	nd	122	nd	36
Min	230	15	33	35	48	69	29	142	3	26	56	20	255	19
Mean	316	72	86	93	1862	211	64	636	16	180	56	81	438	129
Max	410	352	194	167	14710	384	121	5381	42	335	56	171	1300	448

specific source of sulfurs and metals, with oxidation and dissolution of sulfides, hydrolysis, and microbial activity (Sand et al., 2001). These bio-geochemical processes generate acidic sulfate-rich natural springs with high contents in dissolved metals and metalloids. Once the water enters into contact with the riverbed, it begins to interact with low-grade metamorphic rocks (with a slow capacity to neutralize acidity), and with circumneutral tributaries and rivers that dilute and precipitate elements. Under extreme acidity (pH of 2.9), dissolved SO_4^{2-} concentrations exceeding 5000 mg/l, and high amounts of Fe and K^+ (both in the swampy area (RA2) and in the riverbed sediments of the upper catchment), jarosite is the main mineral phase. Supergene jarosite shows relatively slow dissolution kinetics (Baron and Palmer, 1996). On the other hand, schwertmannite dominates in the middle and lower catchment, where the pH increases from 3.4 to 4.5 and the SO_4^{2-} concentrations decrease from <5000–480 mg/l (Fig. 8). The precipitation of the sulfate phases allows metal storage within the bed sediments, and controls the metal distribution in the catchment area. Both in the upper and middle catchment, As, Mo, Cu and Zn accumulation is important. Furthermore, hydrological factors as seasonal variations in freshwater input can play an important role in the spatial and temporal variation of metals concentration. The iron oxides/hydroxides such as hematite, goethite, ferrihydrite, and lepidocrocite would be subordinated or inhibited due to the pH of <4.5, to the high SO_4^{2-} concentrations, and the low amounts of dissolved HCO_3^-. Interestingly, goethite and hematite may be present on the current river terraces as a product of mineral transformation to more stable phases.

Efflorescent sulfate salts occur in both the upper and middle catchment, with three mineral domains: the epsomite salt series, the melanterite group, and the halotrichite-pickeringite group. These three groups are highly soluble and their occurrence is related to evaporation processes in small pools and river channel banks associated with the headwater area. They also play an important role in trace elements retention (eg. Cu, Zn, As, Mo), affecting the metal load in the watercourse. Efflorescent salts reveal the availability of Fe^{+2}, linked to an active sulfur oxidation system or to reducing microbial activity (Nordstrom, 1982; Bigham and Nordstrom, 2000; Murad and Rojik, 2004).

6.2. The paleolacustrine ochre deposits

Specific minerals and high concentrations of iron and other metals in the distal paleolake levels suggest a lake system fed by acid rock drainage through the paleo-Amarillo river. Taking into account the current geochemical characteristics of the Amarillo river and the geological framework of the paleolake strata, an attempt to explain the sedimentological, mineralogical, and geochemical features of the ochres within the distal paleolacustrine facies association through two integrated conceptual models is made: (1) A seasonal controlled cycle, with a change in water composition and river load during alternating summer and winter seasons, and (2) post-depositional changes controlled by particle size, “permeability” variations, and crystallization processes, without significant compositional variations within the lake.

As discussed in the previous section, the conditioning factors of pH and $(SO_4)^{2-}$ determine the mineralogy and geochemistry associated with iron precipitates in the present-day Amarillo river. Moreover, the seasonal variations modify the transport capability of dissolved, colloidal and detrital material. The millimetric thicknesses of the banded ochre facies may correspond to low-stage drainage input (dry winter season), whereas the silty-clay ochre and silty-sandy facies (thicker, lower iron concentrations, and higher detrital phase proportions) would be linked to input during high-discharge periods (wet summer season) and paleoriver flooding events, respectively.

Although the M1, M2, and M3 layers in the banded ochre facies are intimately related in the stratigraphic record, they have distinctive characteristics. The M1 dark brownish colors contrast with the yellowish-orange of M2 and the grayish of M3. The M1 mineralogy of goethite and quartz also contrasts with M2 and M3 which, in addition to these phases, have jarosite, feldspars and clay minerals. The sum of these differences suggests specific physicochemical conditions for the formation of each one. The presence of goethite in this facies is controversial. Under the chemical conditions of the current acid drainage system of the Amarillo river, with pH < 3 in the headwaters and pH ~4.5 in the lower catchment and high $(SO_4)^{2-}$ concentrations all along the basin, the precipitation of iron oxides and hydroxides (goethite) is displaced to iron hydroxysulfates (schwertmannite) (Fernández-Remolar et al., 2005). The

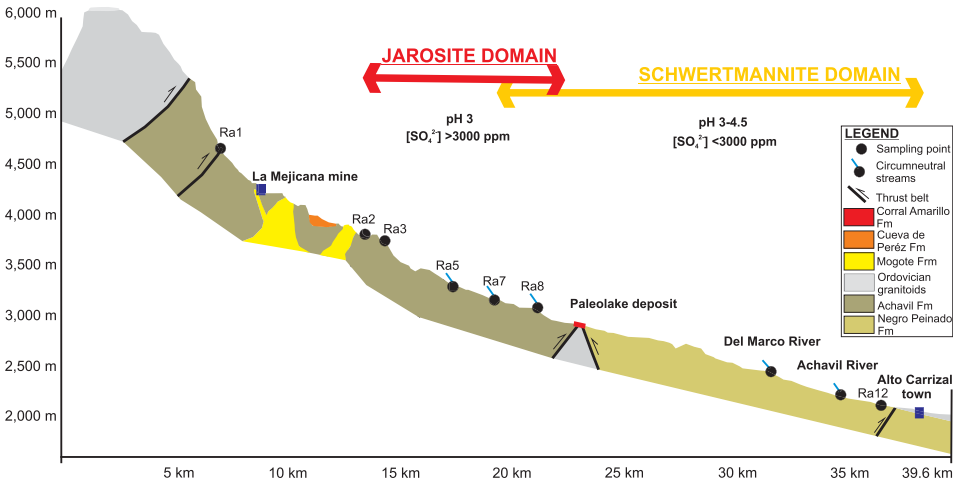

Fig. 8. DEM profile of the Amarillo river representing the spatial domains of jarosite and schwertmannite within the riverbed, which are associated with variations in pH and $(SO_4)^{2-}$.

absence of jarosite in the M1 layer suggests conditions of pH > 3, probably similar to those in the Amarillo river today near RA8 and in the artisanal evaporation ponds (pH 3–4.5 and $(SO_4)^{2-}$ <5000 mg/l), given the location of the paleolake deposits. In this case, goethite could not be a primary mineral (Fig. 9). In the vicinity of sampling station RA8, schwertmannite is the main precipitated phase, but it was not identified in any of the analyzed paleolake layers. However, the progressive transformation of this hydrosulfate into goethite (by aging) has been confirmed. Numerous studies show that this iron hydrosulfate begins to transform into

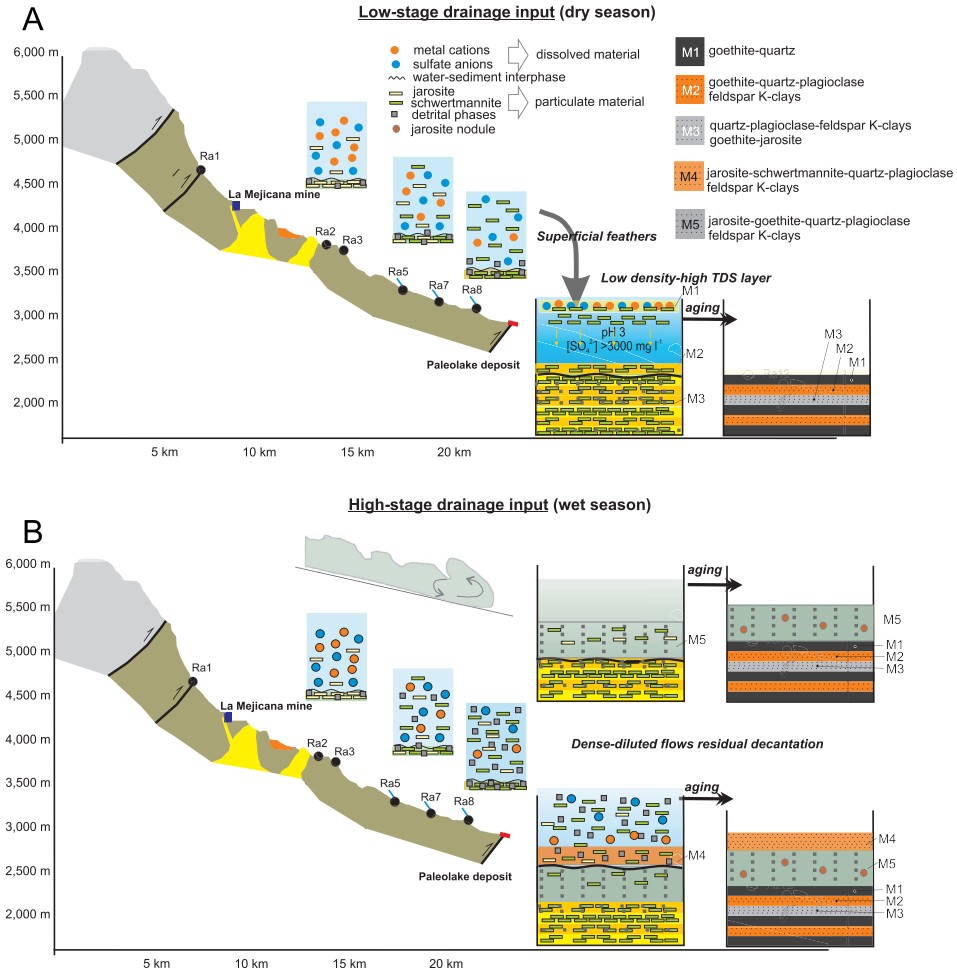

Fig. 9. A) Schematic representation of the formation and post-depositional transformation of the banded ochre facies. B) Schematic representation showing the processes related with the silty-clay ochre facies during the high-flow stage. The post-depositional transformations that caused the appearance of goethite are shown.

goethite and jarosite over timescales of weeks and months as a result of mineral instability (e.g., Bigham et al., 1996; Jönsson et al., 2005; Acero et al., 2006; Knorr and Blodau, 2006).

Assuming the chemical conditions mentioned for the paleolake during the dry season, in which the banded ochre facies would have been deposited, schwertmannite precipitation likely corresponds to stages of minimum detrital material and flow input to the distal lake system. During this season, it is possible that a shallow stream of high TDS acid water could be heated up during daytime hour, reaching higher temperatures than those from the lake. The temperature could be high enough to allow a lower density, high TDS layer formation at the top of the water body, promoting the precipitation and coagulation of colloidal material. As thermal equilibration occurs, the superficial layer would then sink to the bottom generating the M1 layer. M2 and M3 layers could represent initial deposition of the high density material (colloidal and detrital silicates and sulfates, see Fig. 9). Goethite in the M1 layer could be the product of schwertmannite transformation, whereas the absence of jarosite is probably controlled by low sulfate concentrations in solution in the water body and Eh values lower than those required for jarosite stability. It is worth noting that the lake would have been an open system with a loss of water through the detrital barrier damming the valley.

The mineralogy of the silty-clay ochre facies (M4) can be explained as the product of a combination of physical and chemical processes. Minerals such as jarosite, schwertmannite, quartz, plagioclase, and K-feldspar would have been deposited by the residual settling of diluted flows during the wet season, with some associated schewertmannite precipitation. Similarly to what would have happened with the banded ochre facies, goethite contents in the silty-clay ochre facies are likely the product of detrital and precipitated schwertmannite transformation. Additionally, clay minerals and temperature can act as regulators of catalytic transformations of sulfate phases into goethite (Schwertmann et al., 2000). The variable grain size between the three facies could also control the transformation of sulfates into goethite or into goethite + jarosite. The contrast of small jarosite nodules (a couple of millimeters in diameter) in fine sand to silt layers, the change in color in some silty-clay ochre facies (yellowish at the base to gray at the top), along with fine lamination with marked lateral continuity and goethite as the only phase in banded ochre facies (Fig. 3D), all suggest, at least in part, a post-depositional jarosite formation. This formation could be related to acidic pore fluids, linked to capillarity, or related with aging processes, with a better development within the most porous silty-clay ochres and silty-sandy facies. This granulometric model was also proposed to explain alternating goethite and goethite + hematite in fluvial point bars from the ancient terraces of Alto de la Mesa, Río Tinto, Spain (Pérez-López et al., 2011). Goethite crystal size is a limiting factor to produce hematite in later diagenetic steps. High-crystallinity goethite might prevent hematite formation.

It is worth to note that some of the sedimentological features described above could be explained by processes that complement the seasonal cycle and post-depositional processes described above. Seasonal discharge fluctuations would influence primary texture and thus control early diagenetic transformations. Oxidation fronts commonly develop in tailings deposits in arid environments, with the formation of laminated layers with sharp contacts and marked jarosite and/or schwertmannite lateral continuity due to the capillary rise of elements (Dold and Fontbote, 2002). In reducing environments, Fe^{3+} is unstable and is reduced to Fe^{2+}; due to their difference in atomic radius, secondary iron minerals dissolve leaving the iron and sulfur as available mobile elements (Díez-Ercilla et al., 2006). In the present-day Amarillo river terraces dark-brown ochre layers alternate with yellowish layers, presumably produced by capillarity. Moreover, an alternative explanation for precursor schwermannite in the ochre layers (M1) as a product of direct precipitation from the water body would be to link these deposits with meromictic lakes (Boehrer and Schultze, 2008). These lakes are capable of generating water column stratification (~1–5 m) as a result of density variations depending on the concentration of total dissolved solids. The water column stratification would take place during winter, associated with reduced input. However, it should be noted that in the lake deposits no conclusive evidence of anoxia or dysoxia was found in the bottom, which would be expected since sulfides (pyrite-marcasite) should form with iron and sulfur availability (Bigham et al., 1996). However, small limonitic nodules in the deep silty-sandy facies may correspond to expressions of late-oxidized framboids of syngenetic sulfides.

6.2.1. Geochemical interpretation

The metal elements distribution in the paleolake deposits is associated with hydrological annual changes which generate variations in the metals transport load. High contents of iron, sulfate, and metals in the paleolake deposits are associated with their high availability as a result of the oxidative dissolution of pyrite and other sulfides and sulfates (arsenopyrite, enargite, chalcopyrite, alunite, etc.) in the source area, that is, the mineralized zones of the La Mejicana and Nevados del Famatina district. These processes generate acidic and oxidizing waters (low pH and high Eh), enabling the mobilization of relatively insoluble elements. Meanwhile, the Amarillo river hydrological shift from a semi-arid to an arid area could control spatial and temporal variations in metal concentration and partitioning for these elements within the watercourse. During the dry season (winter), the flow has only contribution from the mineralized area and carries large amounts of transition metal elements (mainly in solution but also as colloids) that allow their concentration, as shown in the banded ochre facies. In the wet season (summer), the contribution area (Achavil and Negro Peinado Formations, and granitoids without mineralization) and the transport energy increase and alkaline and alkaline earth elements predominate. They are likely associated with detrital quartz, plagioclase, and K-feldspar, with iron in lower proportions, as shown by the silty-clay ochre facies and the silty-sandy facies.

The distribution of iron contents in the stratigraphic column, both in the M4 and M5 layers, shows a trend with lower concentrations towards the top (Fig. 6). This is, in turn, consistent with a gradual increase in the silty-sandy facies upsequence.

The behavior of trace elements in acid rock drainage is controlled by several factors, such as ore and gangue mineralogy, weathering conditions, and hydrological variations (Jonson and Thornton, 1987; Fernández-Remolar et al., 2011; Monterroso and Macias, 1998a, b; Sanchez-España et al., 2005; Sarmiento et al., 2007). The precipitation of secondary minerals such as goethite, schwertmannite, and jarosite can play an important role in the adsorption and/or co-precipitation of trace elements in solutions. Experimental analysis has shown that large amounts of schwertmannite adsorb As and Mo in a very short time (a matter of hours) due to the behavior of these elements as oxyanions, whereas other divalent trace elements (e.g., Zn, Cu, Pb, Cd, Ni, and Co) are adsorbed to a lesser extent or co-precipitate, requiring more time (Acero et al., 2006; Murad and Rojík, 2005). Therefore, the precipitation of iron hydrosulfates and sulfates (schwertmannite and jarosite) results in the accumulation of significant amounts of metals (such as As, Mo, Cu, Zn, Co, Pb, and Ni) mainly by adsorption or co-precipitation. Several experimental studies show that these concentrations remain constant even after the processes that transform the schwertmannite into goethite are inactive (Schroth and

Parnell, 2005), as it occurs in the present-day Amarillo river and the paleolake deposits.

Moreover, leaching of elements such as Al, K, Na, and Ca from rocks and gangue minerals at low pH could contribute to the formation of clays such as smectites and kaolinite (Fernández-Remolar et al., 2005). Some metals such as Cu, Zn, and Pb, which are abundant in the M5, M4, and M1 layers, could be retained by these clays (Jenne, 1977; Smith, 1999). Under low pH, clay minerals may have highly negative charges that favor the adsorption of positively charged metals (Bowell and Bruce, 1995).

7. Conclusions

The mineralogical analyses (XRD) performed on whole rock and on the <2 μm fraction from distal paleolake deposits within the Corral Amarillo Formation indicate that a rhythmic association is mainly composed of varying proportions of goethite, jarosite, and quartz, with muscovite, biotite, feldspar, chlorite, kaolinite, and smectites as minor components. The geochemical analyses (XRF) carried out on these layers reveal very high and similar contents of Fe_2O_3 and SO_3 concentrations. Other major elements such as SiO_2, Al_2O_3, K_2O, MgO, Na_2O, and CaO show a clear negative correlation with respect to Fe_2O_3, and high concentrations of As, Mo, Cu, Zn, Pb, and Co, are mainly associated with the ochre facies.

The mineralogical analyses (XRD) on samples taken from the present-day Amarillo river catchment reveal three different groups of precipitated sediments associated with acid mine drainage consisting of hydrosulfates, epsomite, and pickeringite-halotrichite melanterite (efflorescent sulfate salts), and jarosite and schwertmannite (bed sediments and dark crusts). Preliminary geochemical studies of bed sediments show high Fe_2O_3 and SO_3 concentrations over the entire catchment with very low SiO_2, Al_2O_3, MgO, Na_2O, and CaO contents. Iron concentrations increase from the headwaters to the lower section, whereas sulfate decreases downstream away from the alteration zone. Some trace elements (such as As, Mo, Cu, and Zn) have very high concentrations in bed sediments and efflorescent salts and tend to decrease downstream. The mineralogical and geochemical distribution of bed sediments can be explained with the model proposed by Cornell and Schwertmann (1996), where the pH and the SO_4^{2-} concentration would be the limiting factors in the precipitation of sulfate/hydrosulfates and the inhibition of iron oxides/hydroxides.

The sedimentary, mineralogical, and geochemical characteristics of the banded ochre facies indicate an association with the paleo-Amarillo river acid drainage (~3483 to 3540 cal a BP). Goethite as the only iron phase is probably a product of schwertmannite early aging. Jarosite in the silty-clay ochre facies has probably a detrital origin but could also be associated with a post-depositional formation conditioned by the chemistry of pore fluids and facies porosity. In turn, high concentrations of iron and other metals and changes in contents between layers would be associated with flow variations during the seasonal cycle. The anomalous values of As, Mo, Cu, Zn, and Pb can be linked to adsorption and/or co-precipitation associated with the formation of sulfates, preserving their concentrations even after their transformation to more stable phases.

Although these acid-oxidizing environments have generally been associated with the interaction between high amounts of sulfide material from exposed tailings and meteoric waters and, therefore, interpreted as genetically polluting processes associated with mining, it is important to note that the Amarillo river paleolake deposits predate mining activity in the region and therefore represent a record of the natural evolution and aggressiveness of these systems.

Acknowledgments

We are grateful to the Consejo Nacional de Investigaciones Científicas y Técnicas (PIP 112-200801-03265 5783 CONICET), the Agencia Nacional de Promoción de Ciencia y Tecnología (PICT-2008-1125; FONCYT), and the Secretaría de Ciencia y Tecnología of the Universidad Nacional de Córdoba (114/07 SECyT-UNC), which support our research projects in western Argentina. Chemical analyses were supported by the Departamento de Mineralogía y Petrología and I.A.C.T., Universidad de Granada-CSIC. We acknowledge Dr. Margarita Do Campo for her help during the fieldwork, and the thorough review by Dr. Karina Lecomte, which helped to improve this work. We would also like to acknowledge the work of Christine Laurin in editing the text and the very constructive reviews and comments by Eduardo O. Zappettini and an anonymous reviewer and the editorial recommendations that allow improving this work.

References

Acero, P., Ayora, C., Torrento, C., Nieto, J.M., 2006. The behavior of trace elements during schwertmannite precipitation and subsequent transformation into goethite and jarosite. Geochim. Cosmochim. Acta 70, 4130–4139.

Asta, A.P., Ayora, C., Román-Ross, G., Cama, J., Acero, P., Gault, A.D., Charnock, J.M., Bardelli, F., 2010. Natural attenuation of arsenic in the Tinto Santa Rosa acid stream (Iberian Pyritic Belt, SW Spain): the role of iron precipitates. Chem. Geol. 271, 1–12.

Astini, R.A., 2003. The Ordovician proto Andean basins. In: Benedetto, J.L. (Ed.), Ordovician Fossils of Argentina. Universidad Nacional de Córdoba, Córdoba, pp. 1–74.

Baron, D., Palmer, C.D., 1996. Solubility of jarosite at 4–35°C. Geochim. Cosmochim. Acta 60, 185–195.

Bigham, J.M., Schwertmann, U., Carlson, L., Murad, E., 1990. A poorly crystallized oxyhydroxysulfate of iron formed by bacterial oxidation of Fe(II) in acid mine waters. Geochim. Cosmochim. Acta 54, 2743–2758.

Bigham, J.M., Schwertmann, U., Carlson, L., 1992. Mineralogy of precipitates formed by the biogeochemical oxidation of Fe (II) in mine drainage. In: Skinner, H.C.W., Fitzpatrick, R.W. (Eds.), Biomineralization Processes of Iron and Manganese: Modern and Ancient Environments. Catena-Verlag, Cremlingen-Destedt, pp. 219–232. Catena Supplement, 21.

Bigham, J.M., Carlson, L., Murad, E., 1994. Schwertmannite, a new iron oxyhydroxysulphate from Pyhasalmi, Finland, and other localities. Mineral. Mag. 58, 641–648.

Bigham, J.M., Schwertmann, U., Traina, S.J., Winland, R.L., Wolf, M., 1996. Schwertmannite and the chemical modeling of iron in acid sulfate waters. Geochim. Cosmochim. Acta 60, 2111–2121.

Bigham, J.M., Nordstrom, D.K., 2000. Iron and aluminum hydroxysulfates from acid sulfate waters. In: Alpers, C.N., Jambor, J.L., Nordstrom, D.K. (Eds.), Sulfate Minerals: Crystallography, Geochemistry, and Environmental Significance, 40, pp. 351–403. Review in Mineralogical and Geochemical.

Boehrer, B., Schultze, M., 2008. Stratification of lakes. Am. Geophys. Union 46, 2006RG000210.

Boult, S., 1996. Fluvial metal transport near sources of acidmine-drainage: relationships of soluble, suspended and deposited metal. Mineral. Mag. 60, 325–335.

Bowell, R.J., Bruce, I., 1995. Geochemistry of iron ochres and mine waters from Levant Mine, Cornwall. Appl. Geochem. 10, 237–250.

Brodtkorb, M.K., Schalamuk, I.B., 1999. Yacimientos de Cobre y Oro de la Sierra de Famatina, La Rioja. Recur. Miner. la República Argent. Inst. Geol. Recur. Miner. SEGEMAR, An. 35, 1495–1505.

Caraballo, M.A., Sarmiento, A.M., Sánchez-Rodas, D., Nieto, J.M., Parviannen, A., 2011. Seasonal variations in the formation of Al and Si rich Fe-stromatolites in the highly polluted acid mine drainage of Agua Agria Creek (Tharsis, SW Spain). Chem. Geol. 284, 97–104.

Collo, G., Astini, R.A., Cawood, P., Buchan, C., Pimentel, M., 2009. U-Pb detrital zircon ages and Sm-Nd isotopic features in low-grade metasedimentary rocks of the Famatina belt: Implications for late Neoproterozoic – early Paleozoic evolution of the proto-Andean margin of Gondwana. J. Geol. Soc. 166, 1–17.

Collo, G., Dávila, F.M., Nóbile, J.C., Astini, R.A., Gehrels, G., 2011. Clay mineralogy and thermal history of the Neogene Vinchina Basin, Central Andes of Argentina: analysis of factors controlling the heating conditions. Tectonics 30, TC4012. http://dx.doi.org/10.1029/2010TC002841.

Cornell, R.M., Schwertmann, U., 1996. The Iron Oxides: Structure, Properties, Reactions, Occurrence and Uses. VCH, Weinheim and New York. ISBN: 3-527-28576-8, 573.

CAA, Código Alimentario Argentino, 1994. Art. 1 Res. MS y AS N°494. Ley 18284. Dec. Reglamentario 2126. Anexo I y II. Marzocchi, Buenos Aires.

Childs, C.W., Inoue, K., Mizota, C., 1998. Natural and anthropogenic schwertmannites from Towada-Hachimantai National Park, Honshu, Japan. Chem. Geol. 144, 81–86.
Dahlquist, J.A., Alasino, P.H., 2005. Hallazgo de granitoides fuertemente peraluminosos en la Sierra de Famatina, orógeno Famatiniano. Rev. la Asoc. Geológica Argent. 60, 301–310.
Dávila, F.M., Astini, R.A., Jordan, T.E., Kay, S.M., 2004. Early Miocene andesite conglomerates in the Sierra de Famatina, broken foreland region of western Argentina, and documentation of magmatic broadening in the south-central Andes. J. South Am. Earth Sci. 17, 89–101.
Dávila, F.M., Astini, R.A., 2007. Cenozoic provenance history of synorogenic conglomerates in western Argentina (Famatina belt): implications for central Andean foreland development. Geol. Soc. Am. 119, 609–622.
De Alba, E., 1954. Descripci6n geológica de la hoja 16c. Villa Unión. Provincia de La Rioja. Servicio Geo1ógico Nacional, Buenos Aires, Argentina. Boletin 82, 83.
Díez-Ercilla, M., López-Pamo, E., Santofimia, E., Sánchez-España, F., 2006. Fotoreducción de Fe (III) en aguas ácidas de mina de la Faja Pirítica. Boletín Geológico Min. 117, 551–556.
Dold, B., Fontboté, L., 2002. A mineralogical and geochemical study of element mobility in sulfide mine tailings of Fe oxide Cu–Au deposits from the Punta del Cobre belt, northern Chile. Chem. Geol. 189, 135–163.
Dold, B., 2010. Basic concepts in environmental geochemistry of sulfidic mine-waste management. In: Kumar, E.S. (Ed.), Waste Management. InTech, Rijeka, Croatia, pp. 173–197.
España, J.S., Pamo, E.L., Pastor, E.S., Reyes, J., Rubi, J.A.M., 2005. The natural attenuation of two acidic effluents in Tharsis and La Zarza-Perrunal mines (Iberian Pyrite Belt, Huelva, Spain). Environ. Geol. 49, 253–266.
Fernández-Remolar, D.C., Morris, R.V., Gruener, J.E., Amils, R., Knoll, A.H., 2005. The Rio Tinto Basin, Spain: mineralogy, sedimentology geobiology, and implication of outcrop rocks at Meridiani Planum, Mars. Earth Planet. Sci. Lett. 240, 149–167.
Fernández-Remolar, D.C., Gómez, F., Prieto-Ballesteros, O., Schelble, R.T., Rodríguez, N., Amils, R., 2008. Some ecological mechanisms to generate habitability in planetary subsurface areas by chemolithotrophic communities: the Río Tinto subsurface ecosystem as a model system. Astrobiology 8, 157–173.
Fernández-Remolar, D.C., Prieto-Ballesteros, O., Gómez-Ortíz, D., Fernández-Sampedro, M., Sarrazin, P., Gailhanou, M., Amils, R., 2011. Río Tinto sedimentary mineral assemblages: a terrestrial perspective that suggests some formation pathways of phyllosilicates on Mars. Icarus 211, 114–128.
Fernández-Turiel, J.L., López-Soler, A., Llorens, J.F., Querol, X., Aceñolaza, P., Durand, F., López, J.P., Medina, M.E., Rossi, J.N., Toselli, A.J., Saavedra, J., 1995. Environmental monitoring using surface water, river sediments, and vegetation: a case study in the Famatina range, La Rioja, NW Argentina. Environ. Int. 21, 807–820.
Gómez, F., Fernández-Remolar, D., González-Toril, E.F., Amils, R., 2004. The Tinto River, an extreme Gaian environment. In: Margulis, L., Miller, J., Boston, P., Schneider, S., Crist, E. (Eds.), Scientist on Gaia 2000. MIT Press, pp. 321–334.
Hermanns, R.L., Strecker, M.R., 1999. Structural and lithological controls on large Quaternary rock avalanches (sturzstroms) in arid northwestern Argentina. Geol. Soc. Am. Bull. 111, 934–948.
Hermanns, R.L., Trauth, M.H., Niedermann, S., McWilliams, M., Strecker, M.R., 2000. Tephrochronologic constraints on temporal distribution of large landslides in NorthWest Argentina. J. Geol. 108, 35–52.
Hermanns, R.L., Niedermann, S., Ivy-Ochs, S., Kubik, P.W., 2004. Rock avalanching into a landslide-dammed lake causing multiple dam failure in Las Conchas valley (NW Argentina) — evidence from surface exposure dating and stratigraphic analyses. Landslides 1, 113–122.
Hermanns, R.L., Folguera, A., Gonzáles Díaz, F.E., Fauque, L., 2006. Landslide dams in the central Andes of Argentina — showing the need of revising the established landslide dam classification. Italian J. Eng. Geol. Environ. 1 (Special Issue), 55–60.
Hudson-Edwards, K.A., Schell, C., Macklin, M.G., 1999. Mineralogy and geochemistry of alluvium contaminated by metal mining in the Rio Tinto area, southwest Spain. Appl. Geochem. 14, 1015–1030.
Jambor, J.L., Blowes, D.W., 1994. Short course Handbook on environmental geochemistry of sulfide mine-Wastes, 22. Mineralogical Association of Canada, Nepean, p. 438.
Jenne, E.A., 1977. Trace element sorption by sediments and soils—site and processes. In: Chappell, W., Peterson, S.K. (Eds.), Proc. Symp. Molybdenum in the Environment. Marcel Dekker, New York, N.Y, pp. 425–552.
Jonson, C.A., Thornton, I., 1987. Hydrological and chemical factors controlling the concentrations of Fe, Cu, Zn and As in a river system contaminated by acid mine drainage. Water Res. 21, 359–365.
Jönsson, J., Persson, P., Sjoberg, S., Lovgren, L., 2005. Schwertmannite precipitated from acid mine drainage: phase transformation, sulphate release and surface properties. Appl. Geochem. 20, 179–191.
Knorr, K.H., Blodau, C., 2006. Controls on schwertmannite transformation rates and products. Geochim. Cosmochim. Acta 70, 4130–4139.
Accepted Lecomte, K.L., Maza, S., Collo, G., Depetris, P.J., 2014. Geochemical dynamics of an acid drainage system: the case of the Amarillo River, Famatina (La Rioja, Argentina). Sci. Total Environ..
Limarino, C.O., Morelli, J.R., Gaidano, D., 1994. Sedimentología y origen del yacimiento Corral Amarillo (Cuaternario), Sistema del Famatina, Provincia de La Rioja. Rev. la Asoc. Geológica Argent. 49, 143–153.
Limarino, C.O., Spalletti, L.A., Colombo Piñol, F., 2010. Evolución paleoambiental de la transición glacial-postglacial en la Formación Agua Colorada (Grupo Paganzo), Carbonífero, Sierra de Narváez, NO argentino. Andean Geol. 37, 121–143.
Losada-Calderon, A., McPhail, D., 1994. The Nevados de Famatina mining district: porphyry- and Epithermal- Style Mineralization, La Rioja Province, Argentina. Actas 7° Congr. Geológico Chil. 2, 1585–1589.
Losada-Calderon, A., Mcbride, S.L., Bloom, M.S., 1994. The geology and $^{40}Ar/^{39}Ar$ geochronology of magmatic activity and related mineralization in the Nevados del Famatina mining district, La Rioja province, Argentina. J. South Am. Earth Sci. 71, 9–24.
Lurgo Mayón, C.L., 1999. Depósitos de molibdeno y cobre diseminados en la Sierra de Famatina, La Rioja. Recur. Miner. la República Argent. SEGEMAR, An. 35, 1495–1505.
Maza, S.N., 2009. Sedimentología, mineralogía y geoquímica de un sistema lacustre Cuaternario de alta montaña en el Famatina y su vinculación con el aporte de drenaje ácido, vol. 73. Universidad Nacional de Córdoba. Trabajo Final.
Maza, S.N., Lecomte, K.L., Collo, G., 2011a. Atenuación natural en un sistema con drenaje ácido asociado a la mina La Mejicana, Famatina, La Rioja. Actas XVIII Congr. Geológico Argent., 1398–1399.
Maza, S.N., Collo, G., Astini, R.A., 2011b. Edad y caracterización geoquímica de la formación Corral Amarillo: Registro de un sistema de drenaje ácido Holoceno en el Famatina. Actas XVIII Congr. Geológico Argent., 1396–1997.
Marcos, O.R., Zanettini, J.C., 1982. Geología y exploración del Proyecto Nevados del Famatina. Servicio Geológico, Secretaría de Minería de la Nación, Buenos Aires. Informe Inédito, 325.
Monterroso, C., Macías, F., 1998a. Procesos de inmovilización de elementos traza en aguas ácidas de mina. Edafología 5, 59–70.
Monterroso, C., Macías, F., 1998b. Aguas de drenaje de mina afectadas por la oxidación de sulfuros. Variaciones estacionales de su composición. Edafología 5, 71–82.
Moore, D.M., Reynolds, R.C., 1997. X-Ray Diffraction and the Identification and Analysis of Clay Minerals. Oxford University Press, p. 378.
Murad, E., Rojík, P., 2004. Jarosite, schwertmannite, goethite, ferrihydrite and lepidocrocite: the legacy of coal and sulphide ore mining. SuperSoil, 1–8. Symposium 1: Acid, sulphate soils.
Murad, E., Rojík, P., 2005. Iron mineralogy of mine-drainage precipitates as environmental indicators: review of current concepts and a case study from the Sokolov Basin, Czech Republic. Clay Miner. 40, 427–440.
Nordstrom, D.K., 1982. The effect of sulfate on aluminum concentrations in natural waters: some stability relations in the system Al_2O_3-SO_3-H_2O at 298 K. Geochim. Cosmochim. Acta 46, 681–692.
Nordstrom, D.K., Alpers, C.N., 1999. Geochemistry of acid mine water. In: Plumlee, G.S., Logsdon, M.J. (Eds.), The Environmental Geochemistry of Minerals Deposits, V6A. Reviews in Economic Geology, Littleton, pp. 133–160.
Pankhurst, R.J., Rapela, C.W., Saavadera, J., Baldo, E., Dahlquist, J., Pascua, I., Fanning, C.M., 1998. The Famatinian magmatic arc in the central Sierras Pampeanas: an early to Mid-Ordivician continental arc on the Gondwana. In: Rapela, C.W. (Ed.), The Proto-Andean Margin of Gondwana Punkhurst, Geological Society of London, Special Publication, vol. 142, pp. 343–367.
Pérez-López, R., Asta, M.P., Román-Ross, G., Nieto, J.M., Ayora, C., Tucoulou, R., 2011. Synchrotron-based X-ray study of iron oxide transformations in terraces from the Tinto-Odiel river system: Influence on arsenic mobility. Chem. Geol. 280, 336–343.
Postma, G., Roep, T.B., 1985. Resedimented conglomerates in the bottomsets of Gilbert-Tipe gravel deltas. J. Sediment. Petrol. 55, 874–885.
Pudack, C., Halter, E., Heinrich, A., Pettke, T., 2009. Evolution of magmatic vapor to gold-rich epithermal liquid: the porphyry to epithermal transition at Nevados de Famatina, Northwest Argentina. Bull. Soc. Econ. Geol. 104, 449–477.
Rogers, D.A., Astin, T.R., 1991. Ephemeral lakes, mud pellet dunes and wind-blown sand and silt: reinterpretations of Devonian lacustrine cycles in north Scotland. Int. Assoc. Sed. Spec. Publ. 13, 199–221.
Sanchez-España, J., López Pamo, E., Santofimia, E., Aduvire, O., Reyes, J., Barettino, D., 2005. Acid mine drainage in the Iberian Pyrite Belt (Odiel river watershed, Huelva, SW Spain): geochemistry, mineralogy and environmental implications. Appl. Geochem. 20, 1320–1356.
Sand, W., Gehrke, T., Jozsa, P.G., Schippers, A., 2001. (Bio)chemistry of bacterial leaching—direct vs. indirect bioleaching. Hydrometallurgy 59, 159–175.
Sarmiento, A.M., Oliveira, V., Gómez-Ariza, J.L., Nieto, J.M., Sánchez-Roda, D., 2007. Diel cycles of arsenic speciation due to photooxidation in acid mine drainage from the Iberian Pyrite Belt (Sw Spain). Chemosphere 66, 677–683.
Schroth, A.W., Parnell, R.A., 2005. Trace metal retention through the schwertmannite to goethite transformation as observed in a field setting, Alta Mine, MT. Appl. Geochem. 20, 907–917.
Schwertmann, U., Friedl, J., Stanjek, H., Schulze, D.G., 2000. The effect of clay minerals on the formation of goethite and hematite from ferrihydrite after 16 years' ageing at 258°C and pH 4–7. Clay Miner. 35, 613–623.
Smith, K., 1999. Metal sorption on mineral surfaces: an overview with examples relating to mineral deposits. Rev. Econ. Geol., 6A, Environ. Geochem. Mineral Deposits, 161–182. Chapter 7.
Taylor, K.G., 1996. Early Cretaceous iron ooids in the Paris basin: pedogenic versus marine origin and their palaeoclimatic significance. Cretac. Res. 17, 109–118.

Trauth, M.H., Strecker, M.R., 1999. Formation of landslide-dammed lakes during a wet period between 40,000 and 25,000 yr B.P. in northwestern Argentina. Palaeogeogr. Palaeoclimatol. Palaeoecol. 153, 277–287.
Trauth, M.H., Alonso, R.A., Haselton, K.R., Hermanns, R.L., Strecker, M.R., 2000. Climate change and mass movements in the NW Argentine Andes. Earth Planet. Sci. Lett. 179, 243–256.
Turner, J.C., 1960. Estratigrafía del tramo medio de la Sierra de Famatina y adyacencias, La Rioja. Boletín la Acad. Nac. Ciencias Córdoba 42, 77–126.
Turner, J.C., 1971. Descripción geológica de la Hoja 15d. Famatina. Secr. Minería, Boletín 126.
Webster, J.G., Swedlund, P.J., Webster, K.S., 1998. Trace metal adsorption onto an acid mine drainage iron (III) oxy hydroxy sulfate. Environ. Sci. Technol. 32 (10), 1361–1368.
WHO, 2004. Guidelines for Drinking-water Quality, third ed. World Health Organization, Geneva.
Wunderlin, C., Maza, S.N., Collo, G., DoCampo, M., Nieto, F., 2014. Caracterización de minerales de arcilla en depósitos asociados a drenaje ácido de roca de la Fm. Corral Amarillo, Famatina. Actas XIX Congr. Geológico Argent. (in press).